行政院國家科學委員會專題研究計畫　成果報告

超音波輔助複合擠製成形之研究(3/3)

計畫類別：個別型計畫
計畫編號：NSC93-2212-E-009-001-
執行期間：93 年 08 月 01 日至 94 年 07 月 31 日
執行單位：國立交通大學機械工程學系(所)

計畫主持人：洪景華

計畫參與人員：洪榮崇、蔡宇中

報告類型：完整報告

處理方式：本計畫可公開查詢

中　華　民　國 94 年 9 月 15 日

中文摘要

超音波塑性加工乃將超音波振動能量作用於成形模具上，經由模具對工件進行成形加工。

本研究計畫預定進行全程三年之研究。在研究中，首先運用有限元素模擬與最佳化分析之系統整合技術，輔助超音波振動成形設備之設計，並製作完成超音波振動成形之實驗裝置。

第二年進行超音波輔助壓縮試驗，研究材料於超音波振動下、材料變形應力降低之現象（Blaha effect）及可能之機制。研究結果顯示，常溫下，附加超音波振動能有效降低鋁合金之壓縮變形負荷；利用不同應變速率進行壓縮試驗，在變形量大時，超音波振動之效果會隨應變速率減小而降低。超音波振動使成形力量降低的機制，應是由應力重疊、差排吸收超音波能量與介面摩擦力降低交互作用產生，非由單一效應所造成。於修正單軸壓縮實驗中，探討超音波振動於壓縮實驗之摩擦的影響，實驗結果顯示，在無摩擦條件下，超音波振動同樣能有效降低鋁合金之壓縮變形負荷。依此推論，超音波振動於壓縮實驗時，材料變形應力降低之機制，實非因介面摩擦降低。其降低塑流應力之主因，應因超音波振動能量施加，使得材料溫度上升影響而降低塑流應力。

經上述的基礎研究後，於第三年中應用在超音波輔助鋁線抽拉及鋁合金端面熱壓的製程上，已獲得顯著的成果。

關鍵詞：超音波振動輔助成形，超音波振動抽拉，有限元素模擬，超音波壓縮試驗

Abstract

Keywords: ultrasonic-vibration assisted forming, ultrasonic-vibration drawing, fine element analysis, ultrasonic-vibration upsetting

The ultrasonic-imposed metal formation processes use ultrasonic energy to act on die then using die to act on workpiece for forming operation.

This project is scheduled to carry on the research of ultrasonic assisted forming for three years. For the first year, the finite elemental analysis and optimization scheme were used to assist the design of experimental apparatus for ultrasonic-imposed metal formation processes. This apparatus has been completed and tested at this stage.

For the second year, a heating device had been designed and manufactured to extend the high-temperature capacity of the above test apparatus. A series of experiments had been conducted with this apparatus to explore the stress reduce effect (Blaha effect) of ultrasonic assisted forming process. Experimental results indicated that ultrasonic-vibration can considerably reduces the compressive forces during hot upsetting. The reducing effect on compressive forces decreases while the temperature increases. The strain rate does not significantly affect the reducing effect on compressive forces. Moreover, the effect of ultrasonic-vibration on hot upsetting cannot be explained by a simple mechanism, such as the effect of interface friction, or superposition of stress, or the absorption by dislocations of the ultrasonic-vibration energy. On the axial compressive tests, the experimental results indicated that under conditions without friction, ultrasonic vibration could still reduce the compressive force of the aluminium alloy effectively. Therefore, evidences concluded that the material temperature raised by ultrasonic vibration energy is the main cause of reducing the flow stress

After above-mentioned basic research, the results were applied to both ultrasonic-vibration auxiliary drawing of aluminum wire and ultrasonic-vibration on hot upsetting of aluminum alloy for the third year. Good results were achieved for both applications.

目　錄

頁次

圖 目 錄

頁次

1. 前言

技術發展，在於因應新工程上要求與新材料應用而進步。新的工程要求，如 IC 封裝用超細線、玻璃骨架用線的製程；新材料，如鈦合金、金屬間化合物等，這些新應用與新材料通常難以加工成形，發展新的製程克服這些難加工成形問題是需要的。超音波加工即是這些有潛力的新製程中，值得開發的一個課題。

超音波加工乃利用頻率產生器內部的振盪電路產生超音波頻率信號，此振盪信號經換能器將電能轉換為機械能，以產生超音波頻率的機械振動。最後利用聚能器與放大器將機械振動的振幅放大，以增加工具加工端的振幅輸出，提升加工效率，如圖 1 所示。一般超音波能量於工業上的應用有：超音波切削、超音波研磨、超音波熔接、超音波洗淨等應用。隨著電子技術的發展與應用，超音波震盪器元件的壓電陶瓷及肥粒鐵磁應變材料出現，使得超音波振動設備的輸出功率獲得相當大的提升。

最近幾年，由於高功率超音波振動設備產生，使得超音波振動塑性加工展現出很大的潛力，此新的製程正在發展克服一些難加工問題。如日本所開發高密度 IC 封裝用之超細銅導線，其線徑可達 15 μm 以下，即利用超音波振動抽拉加工技術製造。而歐美日各國之相關研究機構正積極針對超音波振動於塑性加工的應用進行研究，嘗試發展克服一些難加工成形問題，使得超音波加工技術應用範圍將愈來愈廣。雖然目前已有不少具實效之實驗結果，且為工業界所採用的應用實例亦甚多，但就其超音波振動所產生效應的理論基礎而言，尚存在不少未能測底瞭解之機制。

超音波振動塑性加工與傳統塑性加工之不同，在於前者成形期間，將超音波振動能量作用於成形模具或工件上，經由模具對工件進行成形加工之複合成形。由於超音波振動於塑性加工成形時會產生一些效應，如摩擦力的降低、使材料變形應力降低的效應及成形回彈量的降低現象，使得材料其成形性獲得提高。因此，超音波振動塑性加工能有效達成傳統塑性加工無法達到之加工成形界限，所以超音波於塑性成形之複合加工技術已經逐漸受到重視。

超音波振動作用於塑性加工時，所需之超音波振動能量相當高，為了獲得較高超音波能量，必須針對聚能器（Booster）、振幅放大器（Horn）加以設計，使其共振頻率特性須與頻率產生器之頻率相配合，否則將導致振動系統特性與振動模態改變，影響超音波振動能量傳遞，造成共振頻率偏移、振幅放大率降低、偏振與扭曲模態的出現，振幅分佈不均等現象，甚至造成整個振動系統失效。亦即，聚能器與放大器之選用與設計，將決定整個振動系統之振動特性與效能。

實際應用之聚能器與振幅放大器（喇叭）的形狀有階梯型（Step）、懸鏈曲面形、指數形、錐體形及此四種形狀的各種組合，或依據各種特殊加工要求而設計的形狀如圖 2 所示。振幅放大器的兩端面在相同面積比條件下，其中以階梯形之振幅放大率最大，所以為目前業界最廣用。

隨著 3C 產品之應用與消費者需求下，產品將朝輕、薄、短、小與高級精緻化方向發展。由於金屬機殼具有特殊且高級的質感，且具高散熱性、防電磁波、耐衝擊與高強度等優點，金屬機殼逐漸獲得青睞。目前 3C 產品機殼成形以壓鑄為主，但壓鑄仍有許多無法克服的缺點。而板金沖壓雖具有較佳機械性質、表面精緻、生產速度快、良率高與強度高等

優點，但對於 3C 產品機殼內凸起的螺絲孔（Boss）和肋（Ribs）則無法成形。雖可採用沖鍛成形技術，將螺絲孔與肋之形狀擠製成形，但沖鍛時所需之成形力相當大，降低模具壽命。而超音波振動成形具有降低成形應力之特性，所以超音波振動沖鍛成形將成為 3C 產品機殼之成形的重大技術。

2. 研究動機與目的

如上所述，超音波振動塑性加工能有效達成傳統塑性加工無法達到之加工成形界限，所以目前國外針對超音波振動塑性加工之相關研究，如超音波振動抽拉成形、超音波振動彎曲成形、超音波引伸成形等領域，均有相關研究機構進行研究。但由現有相關研究文獻發現，這些研究多半侷限於常溫成形加工之研究，欠缺對於高溫下超音波振動成形行為之探討。所以，探討超音波振動塑性加工於高溫環境下的成形行為，實有其重要性。

另一方面，目前國內學術界、工業界在超音波應用均局限於超音波檢測、銲接、鑽孔等方面之研究應用，至於超音波振動塑性加工之相關技術研究則甚少相關機構進行研究開發，同時，若欲對超音波振動於塑性加工成形領域進行研究，則由於目前並無商業化的超音波振動成形實驗設備，所以超音波振動成形實驗設備之設計開發亦有其必要性。

因此本研究首先將針對超音波振動頻率產生器、陶瓷壓電振動換能器、振幅放大器及振動成形模具設計規劃，並利用有限元素模擬分析輔助設計，建立振幅放大器設計之模擬模型，達成振幅放大器之設計製作及模具之振動模式，並利用冷卻系統克服超音波設備於高溫下運作之困難點，開發完成一套超音波振動高溫成形之實驗設備。最後藉由開發完成之實驗設備，進行超音波振動高溫成形之相關研究與應用，同時應用有限元素法模擬分析，進行超音波振動抽拉成形模擬，找出適當製程參數；利用實驗結果來驗證模擬結果，建立有效之模擬模型。

在超音波成形的材料上，本研究選擇常用之鋁合金，利用上述開發完成之實驗設備，進行超音波振動高溫成形相關研究；最後進行修正壓縮實驗與環壓縮實驗，探討超音波振動於壓縮實驗時，對介面摩擦的影響。

3. 文獻回顧

將超音波振動能量應用於金屬之塑性行為研究，最早由 Blaha 與 Langenecke【1】所提出，他們對單晶鋅試片進行拉伸試驗時，附加一超音波振動於負荷上，實驗結果發現超音波振動作用時，材料之降服應力會產生降低現象，如圖 3 所示。且金屬在塑性成形時，其材料變形流動應力大為減少，此現象稱為 Blaha effect。後來 Langenecke【2】又針對鋁、銅、鋼等多晶材料進行超音波在金屬變形特性的影響，實驗證明超音波振動能量增加，材料塑流應力隨之降低，且認為以差排理論與機械波動理論無法合理去解釋超音波應力波與差排之互相影響，因此他只針對實驗結果現象作一些描述與預測。對於降低塑流應力的原因，Nevill【3】不認同 Kempe 等人所提出的差排吸收振動能量的三種可能機制假設：（1）共振機制（2）鬆弛機制（3）遲滯機制。認為變形流動應力降低是由於靜態應力和交變應力交互作用產生，因此提出應力重疊機制之假設。所以 Blaha effect 之機制至今尚未有普為接受

之理論解釋。

Pohlman【4】則是最早進行超音波振動對於摩擦力影響之研究，利用如同唱針於唱片之旋轉台裝置，測試超音波對摩擦力之影響。如圖 4 所示，將一個球放置於迴轉平板以不同方向施加超音波振動，實驗得到當振動體的接觸面在振動方向與摩擦力方向平行，且在最大振幅時，降低之摩擦力最大。Siegert【5】則對超音波振動作用下，金屬成形摩擦的可能影響及成形部份之表面品質改善進行研究。由實驗結果，認為振幅與抽拉速度為降低摩擦力主要影響參數，對於表面粗度的改善，同樣受抽拉速度及振幅之影響。Lucas【6】則利用振動的適應性與靈敏度分析技術去評估模具超音波模態，進行超音波振動模具改良設計。

目前應用超音波振動於塑性成形加工之研究，在抽拉成形加工方面，Severdenko【7】【8】將超音波振動應用於鈦、鎳合金、不銹鋼之線材抽拉與超音波徑向振動對抽拉模具幾何形狀影響之研究，研究發現超音波振動所需的抽拉力減少，其原因並非只有摩擦力降低所導致，尚有塑性變形阻力的降低。而超音波振動作用時，模具角半徑小時，提高的極限抽拉比較大。Siegert【9】將超音波振動應用於線材抽拉成形之研究，研究中以徑向超音波振動方式探討抽拉速度及振幅對於抽拉應力之影響，實驗證明由於超音波振動的作用使得抽拉力減少、抽拉速度可較傳統抽拉快，因此適當控制抽拉力、振幅及抽拉速度，可以達到傳統抽拉成形無法達到之材料成形界限。Murakawa【10】同樣對超音波振動於線材抽拉成形進行研究，分別對傳統抽拉（CD）、軸向超音波振動抽拉（AVD）及徑向超音波振動抽拉（RVD）實驗比較，藉由不同潤滑劑、振幅探討工件之表面條件及抽拉力來評估潤滑劑的選用，並對CD、AVD和RVD其頻率、振幅與臨界抽拉速度之關係。超音波置於金屬塑性成形時，材料變形之阻力大為降低，而成品之品質與精度均相對提高。Hayashi【11】提出一新的超音波振動線材抽拉成形方法，利用兩個分裂模具，分別施加超音波振動進行圓形與方形線材抽拉成形，實驗結果得到經由此方法抽拉成形的線材表面不會產生氧化層，其表面性質完整且形狀精密度高。

在板材彎曲成形方面，Tsujion【12】【13】將超音波振動應用於金屬板彎曲成形，研究中以V形彎曲振動模具對金屬板進形彎曲實驗，實驗發現當靜壓力相同下，超音波之振幅增加其金屬板可彎曲角度隨之增加，且金屬板之回彈角度減少。另外也對超音波振動於彎曲成形時之加工硬化、彎曲表面粗糙度及曲率半徑影響之研究，並證明超音波振動下，使加工硬化、彎曲表面粗糙度降低而彎曲部份之曲率半徑增加。在深引伸成形方面，Jimma【14】將超音波振動應用於軸對稱之板材深引伸，研究中在超音波振動作用下，可使304不銹鋼之極限引伸比（LDR）由2.38增加至2.77，超越了沒有摩擦之理想模具深引伸時，極限引伸比（LDR）為2.7之理論值的界限。而造成LDR的提高原因，乃由於超音波振動使得摩擦減少及變形阻力降低（Blaha effect）。Jin【15】則將超音波振動應用於管材抽拉、引伸成形，研究中對不同潤滑劑在徑向振動作用時之影響，並對超音波振動在極限壁厚減縮比間影響、成形精度和表面粗糙度進行探討，驗證在超音波振動下，極限壁厚減縮比、成形精度、提高，且表面粗糙度降低。

而運用有限元素法對超音波振動於塑性成形之模擬分析方面，則有Petruzelka【16】利用VISIOPLAST這套軟體對超音波振動於管材抽拉成形進行模擬分析，研究中以插塞位置在縱向超音波振動波形之固定振動回路振動節點、反節點及非節點位置，分析抽拉期間傳統與有超音波振動其材料流動率、變形率、變形、應力及塑性力分佈改變較大之區域。Jin

【17】則利用DEFORM-2D和DEFORM-3D對超音波振動線材抽拉成形進行模擬分析，研究中以徑向超音波振動抽拉（RUVD）及橫向超音波振動抽拉（TUVD）模擬分析，模擬結果其抽拉力和加工硬化的減少、抽拉線內部之應力與應變分佈均與實驗值接近。

另一方面，Huang【18】在端面壓縮試驗中，將超音波振動以同軸方向作用在成形模具上，並以塑膠黏土替代高溫金屬進行實驗，模擬金屬於高溫下超音波振動成形行為，實驗結果證實材料成形阻力明顯降低，並推測其原因為應力疊置以及超音波作用的介面溫度上升，使摩擦係數改變，進而降低介面摩擦力。

4. 研究方法

超音波塑性加工乃利用超音波振盪器產生電力的振動能，經由壓電陶瓷換能器將電力振動能轉變為機械的振動能，並將超音波振動能量作用於成形模具上，經由模具對工件進行成形加工之成形技術。由於超音波振動於塑性加工成形時會產生一些效應，如摩擦力的降低、使材料變形應力降低的 Blaha effect 及板金成形回彈量的降低等等效應，使得材料其成形極限之界線獲得提高。而影響這些效應則有抽拉速度、超音波頻率、振幅大小與分佈、振動方向、振動位置等變數。因此本研究分為三個階段進行，首先將進行超音波振動高溫成形實驗設備之設計開發，超音波振動成形實驗設備主要構成包括超音波振動頻率產生器、換能器、振幅放大器、成形振動模具等，計畫中將針對這些部份進行設計研究。並利用有限元素模擬分析輔助設計，建立振幅放大器之設計模型，達成振幅放大器之設計製作及模具之振動模式，並建立加熱裝置，利用冷卻系統克服超音波設備於高溫下運作之困難點，開發完成一套超音波振動高溫成形之實驗設備。

第二階段則藉此實驗設備建立金屬於超音波振動之材料塑性成形特性及對這些效應進行基礎研究的探討，進行超音波振動壓縮試驗，探討材料於超音波振動下，會產生摩擦力減少、材料變形阻力降低（Blaha effect）、材料之物理與機械性質變化、材料溫度上升等現象之研究。進行超音波振動高溫端面壓縮實驗，探討超音波振動對鋁合金於端面壓縮實驗影響與在不同溫度、應變速率之間的關係，嘗試建立金屬在超音波振動下材料之塑性特性研究及進行可能機制的探討。由於超音波振動製程現象在高速發生，藉由傳統實驗分析去理解其改善機制是很困難。

所以，第三階段則為實際進行超音波塑性加工成形應用，研究中擬以超音波振動抽拉成形為載具，並以有限元素法進行超音波振動成形模擬分析，嘗試去瞭解超音波振動成形改善的機制。模擬分析時需要材料的基本性質，如應力-應變曲線、介面摩擦係數等。其中應力-應變曲線可由端面壓縮實驗得到，而介面摩擦係數將由圓環壓縮實驗求得。於應用有限元素法模擬分析中，本研究，在完成初步模擬模型後，將以不同的製程參數進行控制變數模擬，如振幅大小、抽拉速度等變數，觀察其交互間的影響及對成形力與製成品的影響。找出適當製程參數；利用實驗結果來驗證模擬結果，建立有效之模擬模型。

5. 結果與討論

5.1. 放大器之最佳化設計結果

本研究中結合有限元素分析與最佳化設計，應用有限元素軟體 ABAQUS／STANDARD 以及最佳化程式 MOST 開發系統整合技術，嘗試對目前業界較廣用之階梯形放大器進行最佳化設計，提供一精準快速且自動化之振幅放大器最佳化設計系統。

1. 收斂曲線

本研究目的乃建立有限元素與最佳化之整合技術，初步以單一變數問題進行研究，藉此建立完整的振幅放大器最佳化設計之整合流程，由簡單階級形放大器之雙變數最佳化結果。經最佳化整合可得到振幅放大器之最大放大率因子 M = 2.658，其收斂曲線，如圖 5 所示。最佳化設計變數 X1 = 64.07645 mm，X2 = 56.45947 mm，其收斂曲線，如圖 6 所示。

2. 理論近似解曲線

由基本理論得知，階級型放大器之大小斷面積比為常數時，其振幅放大率隨大小斷面之長度比而改變。且當長度比為 1 時，振幅放大率為最大，如圖 7 所示。由圖中可知最大振幅放大因子為 2.78，雖然大於模擬最佳化解之 2.658，但由實驗結果證明，由有限元素分析與最佳化系統整合所得之最佳解，較理論近似解更接近實驗值。且最大振幅放大因子，並非發生在大小斷面之長度比率為 1 時。

研究中，已建立完成以程式語言將有限元素分析軟體 ABAQUS 與最佳化程式 MOST 進行系統整合技術，提供一精準快速且自動化之振幅放大器最佳化設計系統。同時確實完成超音波振動壓縮試驗裝置之設計製作，並建立完成超音波振動加熱裝置與冷卻系統，如圖 8 所示。

5.2. 超音波振動於鋁合金高溫端面壓縮實驗

5.2.1. 超音波振動和溫度於端面壓縮之影響

圖 9 為溫度 25°C 時，以真應變速率 0.03 1/s，進行傳統端面壓縮(CU)與軸向超音波振動端面壓縮(AUU)實驗結果之負荷位移比較圖，圖 9（a）所示，當 CU 在壓縮率 67%（位移 4mm）時，壓縮力約 1511 kg，而 AUU 在相同壓縮率時，壓縮力為 1296 kg，壓縮力較 CU 降低 215 kg，此實驗結果證實在超音波振動作用下，可有效降低材料塑性變形應力。圖 9（b）顯示，在超音波振動作用下，隨著壓縮率增加，其變形阻力的降低亦隨之增加，即超音波振動降低變形阻力效應隨壓縮率增加而增加。

圖 10 為溫度 100°C 時， CU 與 AUU 實驗結果之負荷位移比較圖，由圖中所示，CU 在壓縮位移量 4mm 時，壓縮力為 1317 kg，因材料隨溫度升高會降低變形應力，所以壓縮力較 25°C 降低 194 kg。而 AUU 在相同壓縮量時，壓縮力降為 1165 kg，壓縮力較 CU 減少 152 kg。但對降低材料變形阻力之效應較 25°C 減少 63 kg。

圖 11 為溫度 200°C 時， CU 與 AUU 實驗結果之負荷位移比較圖，由圖中所示，CU 在壓縮位移量 4mm 時，因溫度上升使壓縮力降為 1161 kg，其壓縮力較 25°C 時降低 350 kg。而 AUU 在相同壓縮率時，其壓縮力降為 1014 kg，壓縮力較 CU 降低 147 kg。雖然降低了材料塑性變形阻力，但降低的數值與溫度 100°C 時相當接近。

圖 12 為溫度 250°C 時，CU 與 AUU 實驗結果之負荷位移比較圖。圖 12（a）所示，當 CU 壓縮位移量 4mm 時，壓縮力降為 1040 kg，其壓縮力較 25°C 降低 471 kg。而 AUU 在相同壓縮量時，壓縮力為 885 kg，壓縮力較 CU 降低 155 kg，但降低的壓縮力與溫度 100°C 、200°C 時相當接近。圖 12（b）顯示，因超音波振動作用所降低的壓縮力，亦隨著壓縮率增加而增加。

溫度與超音波振動之間關係，可由圖 13 發現，當 25°C 、100°C 時 AUU 之負荷，分別相當於 CU 在溫度 100°C 、200°C 時之負荷。即超音波振動所降低塑流應力之效應，與溫度升高 100°C 所降低塑流應力之效應相當。但壓縮位移低於 3mm 時，超音波振動產生效應高於升溫 100°C 所產生效應。

圖 14 為真應變速率 0.03 1/s，分別以溫度 25°C 、100°C 、200°C 、250°C 進行 CU 與 AUU 之實驗結果比較圖。圖 14（a）與（b）顯示隨溫度上升，CU 與 AUU 之壓縮力均隨之降低。圖 14（c）為各溫度之下，因超音波振動效應所降低的壓縮力位移比較圖。在溫度 25°C 時，超音波振動降低壓縮力效應最佳。而隨溫度升高，超音波振動所產生的降低變形阻力效應反而降低。

5.2.2. 超音波振動和應變速率於端面壓縮之影響

研究中，以真應變速率為 0.03 1/s 與 0.003 1/s 兩種實驗條件下，分別以溫度 25°C 、100°C 、200°C 、250°C 進行 CU 與 AUU 實驗。圖 15 顯示，溫度 25°C 時，應變速率對 CU 與 AUU 均沒有顯著影響。圖 16 得知，CU 與 AUU 在 0.003 1/s 時，相較於 0.03 1/s 時之負荷均有顯著減少。顯示在高溫時，不論有無附加超音波振動，應變速率對於材料之流動應力影響相當大，且應變速率越慢，其變形應力越小。

圖 17 為 CU 在各溫度下，真應變速率 0.03 1/s 與 0.003 1/s 兩者壓縮力相差值與位移比

較圖。其中壓縮力差值(F_d)定義如下：

$$F_d = F_{\dot{\varepsilon}=0.03} - F_{\dot{\varepsilon}=0.003} \tag{4.1}$$

式中$F_{\dot{\varepsilon}=0.03}$為真應變速率 0.03 1/s 之負荷，$F_{\dot{\varepsilon}=0.003}$則為真應變速率 0.003 1/s 之負荷。

圖 18 為 AUU 在各溫度下，真應變速率 0.03 1/s 與 0.003 1/s 兩者壓縮力相差值與位移比較圖。由圖中顯示，在溫度 250$^{\circ}C$時，應變速率則對壓縮力產生極大影響，且應變速率越慢，其壓縮力則越低。另外當溫度在 25$^{\circ}C$、100$^{\circ}C$時，且壓縮位移量超過 3mm，相差壓縮力值則開始轉為負值。初步推論造成塑性應力升高原因，由於超音波振動系統會隨發振時間增加而使振動系統各元件溫度升高，以致能量轉換效率降低，所以輸出振動能量隨時間增加而減少。

5.2.3. 超音波振動於高溫端面壓縮之機制

依文獻，超音波振動可能產生機制有，(1)降低材料變形流動應力。(2)摩擦力降低。(3)溫度上升。在降低材料塑流應力之原因：一般認為可能為，(1)差排因共振吸收能量而克服能障。(2)差排自外加週期應力吸收能量而脫離束縛能障。(3)材料內摩擦效應。(4)靜態應力與交變應力的應力重疊效應。而超音波振動應用於金屬塑性加工所產生的效應相當複雜。除降低塑流應力外，還需考慮摩擦效應與材料溫度上升。如抽拉與引伸時，其摩擦效應較為顯著。

本研究主要針對超音波振動於高溫端面壓縮的影響，經由實驗結果初步推論，在此製程中，因一般差排環的自然頻率約為 100 MHz【19】，研究中超音波頻率為 20 kHz，所以差排因共振吸收的能量小，對於塑流應力降低影響不大。由圖 9（b）所示，超音波振動效應所降低壓縮力隨變形量增加而增加，若超音波振動所造成塑流應力降低是由應力重疊的效應，其降低的壓縮力應為定值，且不會隨變形量增加，所以推論塑流應力的降低不是只有應力重疊機制。

由圖 14（c），超音波振動效應所降低壓縮力隨溫度增加而減少。初步推論其原因：(1)材料在高溫下潛變特性逐漸增加，變形機構與常溫時不太相同，其變形應力隨溫度升高而降低。所以超音波振動作用時，隨溫度升高其熱彈性效應亦隨之減少，以致超音波振動能量被材料吸收降低，造成超音波振動效應降低原因。(2)超音波振動使模具與試片間之介面局部溫度升高，超音波能降低之摩擦力效應減少。

實驗結果，不同之應變速率對於超音波振動降低材料塑流應力之效應，沒有顯著的影響。由於受限於超音波振動設備無法長時間運作，目前本研究只能進行兩種應變速率之實驗。因此超音波振動與應變速率相依性尚無定論。在未來研究中，將針對更多應變速率實驗，進一步探討超音波振動與應變速率之關係。

5.3. 超音波振動於端面壓縮之摩擦影響

當進行單軸壓縮試驗時，由於試片與上下壓板接觸介面間摩擦之影響，使得試片兩端

面受到侷限，以致試片介面材料徑向流動受到抑制，因此產生如圖 19 所示，較不易塑流變形之斜線區域，造成試片產生桶狀之外形。所以於此條件下所得到為非均勻變形之應力、應變曲線，其中包含摩擦影響之因素。為使摩擦影響因素降至最低，本研究採用較為廣泛的修正單軸壓縮試驗。

實驗中之試片分別為具有相同直徑 6mm、高度不同的鋁合金圓柱體，其直徑高度比 d_0/h_0 分別為 2、1.5、1 三種，且於試片兩端噴上二硫化鉬之潤滑劑如圖 20 所示。實驗方法為施加一固定壓力負荷於試片上，除去負載後量取實驗後試片高度，實驗條件為改變不同的固定壓力負荷，分別依序針對不同直徑高度比之試片重複以上步驟實驗。最後將所得實驗數據整理，如圖 21（a）所示。將相同負荷條件下，對不同直徑高度比之試片產生的工程應變，以線性趨近畫一直線。由圖可知當 d_0/h_0 之比值為零時，此試片之高度可視為無限大，因此端面受摩擦力的影響將非常小，所以試片之整體變形可視為均勻壓縮變形。

圖 21 分別為傳統單軸壓縮試驗與超音波振動單軸壓縮試驗之端點效應修正圖。圖 21（a）所示，以 500kg、800kg、1100kg、1500kg 及 1800kg 等五種固定壓力負荷，針對 2、1.5、1 三種不同直徑高度比實驗結果，由圖中可知，將線性趨近直線以外插方法，即可求得當 d_0/h_0 之比值為零時各負荷下之應變。圖 21（b）所示，為 500kg、800kg、1100kg 及 1500kg 等四種固定壓力負荷，針對 2、1.5、1 三種不同直徑高度比之超音波振動實驗結果。由於超音波振動單軸壓縮時，壓縮負荷 1500kg 時，d_0/h_0=1 試片其真應變已高達 56.24%，所以採用四種固定壓力負荷。

圖 22 為傳統與超音波振動修正單軸壓縮實驗結果比較圖，圖中所示資料點，均由端點效應修正圖，經過外插修正得到 d_0/h_0 為零時之真應力-應變圖。當傳統單軸壓縮之施加壓縮負荷為 1800kg 時，其真應變量為 57.59%，而真應力為 357.91Mpa。而當超音波振動單軸壓縮之施加壓縮負荷為 1500kg，其真應變量反而增加為 60.29%時，而真應力降則降為 290.3Mpa。由此實驗結果顯示，當將端面摩擦力影響之效應降到為零，超音波振動作用下，仍能有效降低材料塑性變形應力。而先前所探討超音波振動產生機制時，認為摩擦力降低之效應，可能為降低材料塑流應力原因之一。但由修正壓縮實驗結果顯示，在無摩擦力影響下，超音波振動作用下，仍能有效降低材料塑性變形應力。由此推論，於超音波振動端面壓縮成形時，超音波振動產生降低摩擦力的效應很小。

圖 23 為傳統單軸壓縮試驗於不同直徑高度比時之真應力-應變比較圖，圖中所示，當施加 1800kg 之相同壓縮負荷，直徑高度比 $d_0/h_0=2$ 之試片，其真應變為 45.05%時，真應力為 405.7Mpa，而直徑高度比 $d_0/h_0=0$ 的試片，其真應變為 57.59%時，真應力為 357.9Mpa，真應力較 $d_0/h_0=2$ 明顯降低。此實驗結果顯示，相同壓縮負荷條件下，試片之直徑高度比 d_0/h_0 增加，材料塑流應力隨之增加，且壓縮應變量隨之減少。依推論其原因，應由於直徑高度比 d_0/h_0 增加，以致端面摩擦影響的效應增加所造成。

圖 24 為超音波振動單軸壓縮試驗於不同直徑高度比時之真應力-應變比較圖，圖中所示，當施加 1500kg 之相同壓縮負荷，相同振動條件，直徑高度比 $d_0/h_0=2$ 之試片，其真應變為 48.06%時，真應力為 328.08Mpa，而直徑高度比 $d_0/h_0=0$ 的試片，其真應變為 60.3%時，真應力為 290.3Mpa，其實驗結果與無施加超音波振動之趨勢非常相似，依然存在端面摩擦影響的效應，不因超音波振動作用而減少。再次驗證超音波振動端面壓縮成形時，產生降低摩擦力的效應很小。

5.4. 超音波振動線材抽拉之有限元素模擬分析

5.4.1. 抽拉速度與抽拉力之影響

圖 25 為傳統抽拉（CD）在不同抽拉速度之抽拉力模擬結果圖，如圖所示，無論抽拉速度為何，其抽拉力均約為 620 N (σ =23.5 N/mm$^{2)}$)，其中抽拉力有約 60-80 N的變動，應是有限元素模擬的計算誤差。

圖 26 為軸向超音波抽拉（AUD）的模擬結果圖，如圖 26（a）所示，抽拉速度為 30 mm/s時，其抽拉力約為 450 – 670 N區間內變動，且隨超音波之振動週期(67 μs)變動。圖 26（b）為抽拉力變動週期的詳細圖。當抽拉速度超過臨界抽拉度速度，以V_d=300 mm/s之速度時，則如圖 26（c）所示，其抽拉力與CD所得到 620 N幾乎相同。此說明超過臨界抽拉速度時，抽拉力因超音波振動而變動之原因將消失。

最後，有關於徑向超音波抽拉（RUD）之模擬，如同先前模擬方法。模擬結果如圖 27 所示，由圖 27（a）得知，抽拉速度為 30 mm/s時，其抽拉力約為 280 – 580 N區間內變動，且隨超音波之振動週期(67 μs)變動。緊接著若以抽拉速度為 300 mm/s時，其抽拉力之變動則約在 400 – 620 N區間，然而，當抽拉速度高達V_d=1000 mm/s之速度時，模擬之抽拉力與CD所得到 620 N幾乎相同。由模擬結果可得以下結論，於AUD和RUD兩種情況下，其抽拉速度低於臨界抽拉速度時，抽拉力伴隨模具振動週期而變動，且變動振幅隨抽拉速度減少而增加。當抽拉速度接近臨界值時，抽拉力的變動則將消失。

5.4.2. 實驗與有限元素模擬之抽拉速度和抽拉力關係比較

如同上面所描述，經由實驗所量測的抽拉力，依推論應是由於超音波振動所產生實際變動抽拉力的平均值。圖 28 為 CD、AUD 和 RUD 之抽拉速度與抽拉力關係圖，依照模擬結果，在 CD 其平均抽拉力與抽拉速度無關，且與實驗得到的結果一樣，抽拉力均為 620 N。至於 AUD 時，由抽拉力曲線改變的區分點，即為臨界抽拉速度，其值為 93.6 mm/s，當抽拉速度為臨界速度或更高時，其曲線與 CD 之曲線相似。另一方面，當抽拉速度低於臨界速度，抽拉力有隨抽拉速度的減少，而趨向於零的傾向。對於 AUD 和 RUD 而言，抽拉力的傾向幾乎相同，然而 RUD 的臨界抽拉速度約為 AUD 的十倍。換言之，研究中模擬分析所描述的抽拉速度與抽拉力的關係，其結果與傳統實驗所得到結果相同。

5.4.3. 超音波振動的振幅與抽拉力之關係

根據臨界速度的觀念，可經由增加超音波振動的頻率或振幅來得到很大抽拉力的減少，由高速的抽拉速度所產生的效應，就生產力而言是有幫助。

由以上所觀察到的現象，我們應用有限元素模擬，模擬當振幅較先前的實驗高 10 倍時(i.e., a=10 μm)，其抽拉力的波形。模擬分析在高振幅其抽拉力的理由，主要因為超音波振動裝置的特性，增加振幅比增加頻率容易。而且，在 15 kHz 的振動頻率下，10 μm 的振幅實際上是可以達到。

圖 29 為兩種抽拉速度進行 AUD 之模擬分析抽拉力的結果圖，根據結果，抽拉力的變動由於超音波振動的改進，大約為圖 26 所示結果的十倍。

圖 30 為 RUD 時，以三種不同抽拉速度所模擬分析的抽拉力波形。在同樣 AUD 例子，

抽拉力的變動區間較圖 27 所示結果有所改善。特別在抽拉速度為 300 mm/s 或較少時，其抽拉力的下限為零，這意思表示模具從線材完全分離。換言之，RUD 於抽拉前進的前提下，其模具和線材重複接觸和分離的過程，可經由有限元素模擬分析定量驗證。

圖 31 為 10 μm 的振幅時，CD、AUD 和 RUD 之頻率平均抽拉力，因此，其有關結果討論類似圖 12 所討論，當抽拉速度低於或等於 AUD 與 RUD 的臨界抽拉速度，抽拉力基本上減少且趨近零。而且，有限元素分析預測，RUD 其抽拉速度高達 8900 mm/s 時，依然有振動效應。

6. 結論

本研究是以有限元素模擬分析，搭配理論推導與經驗公式進行換能器、聚能器與放大器之設計，建立完成高溫環境下超音波振動成形之實驗裝置。並建立應用有限元素軟體 ABAQUS／STANDARD 及最佳化程式 MOST 系統之整合技術。提供一精準快速且自動化之振幅放大器最佳化設計系統。且進一步探討超音波振動在不同溫度與應變速率下，對鋁合金端面壓縮的影響。由研究結果可得一些結論如下：

實驗設備製作方面：

1. 證實超音波振動系統於高溫環境下運作之可行性。
2. 高溫端面壓縮實驗中，爐內溫度與試片溫度相差甚大，必須於模具設計加熱裝置，進行溫度補償。
3. 建立完成高溫環境下超音波振動成形之實驗裝置。

數值模擬分析與最佳化：

1. 實驗證明，研究中所建立之有限元素分析模型能縮短振幅放大器設計製作時間，且有效預測共振頻率與振幅分佈。
2. 建立完成有限元素模擬分析與最佳化系統之整合技術。提供一精準快速且自動化之振幅放大器最佳化設計系統。
3. 由有限元素分析與最佳化系統整合所得之最佳解，較理論近似解更接近實驗值。

超音波振動於鋁合金高溫端面壓縮實驗：

1. 實驗證明，軸向超音波振動能有效降低高溫端面壓縮時成形力量。
2. 高溫端面壓縮實驗中，超音波振動使成形力量降低的機制，由應力重疊、差排吸收超音波能量與介面摩擦力降低交互作用產生，非由單一效應所造成。
3. 超音波振動降低高溫端面壓縮時的成形力量，隨溫度升高而減少。

應變速率對超音波振動降低材料塑流應力效應影響不大。

超音波振動於端面壓縮之摩擦影響：

1. 實驗證明，在無摩擦力影響之效應下，超音波振動作用，仍能有效降低材料塑性變形應力。
2. 超音波振動端面壓縮中，對於改善端面摩擦影響的效應很小。
3. 超音波振動端面壓縮成形時，超音波振動使成形力量降低的機制中，降低摩擦力效應的影響很小，故此效應可排除。

超音波振動線材抽拉之有限元素模擬分析：

1. 建立一個徑向超音波抽拉與軸向超音波抽拉時，抽拉力波形之定量分析方法，證明

抽拉力波形隨著超音波振動的週期而改變。

2. 由 FEM 分析所得到的臨界抽拉速度與理論值想當一致，且與實驗結果得到的抽拉速度相的符合。
3. AUD 和 RUD 之抽拉力波形變動的頻率平均值與實驗抽拉力量測結果非常一致。
4. 由有限元素的定量分析驗證抽拉速度隨振幅減少而降低。

建議：

1. 由於受限於超音波振動設備輸出功率，且無法長時間運作，以致於超音波振動成形無法廣泛應用，如成形應力需大的擠製、鍛造成形製程。目前本研究只能進行壓縮、衝壓之實驗。因此在未來研究中，將尋求更高功率，且運作時間長之超音波振動產生設備，進一步探討超音波振動成形之應用。
2. 超音波振動應用於金屬塑性加工所產生的效應相當複雜。除降低塑流應力外，還需考慮摩擦效應與材料溫度上升。且超音波振動製程現象在高速發生，藉由傳統儀器實驗量測分析去理解其改善機制是很困難，因此需尋求適當的量測儀器與方法進行量測分析。

7. 參考文獻

1. F. Blaha, and B. Langenecker, Naturwissenschaften, 1955, v.42, pp. 556.
2. B. Langenecker, “Effects of ultrasound on deformation characteristics of metals”, IEEE Transactions on Sonics and Ultrasonics, 1966, v.13, pp. 1-8.
3. G. E. Nevill and F. R. Brotzen, “The effect of vibration on the static yield strength of low-carbon steel”, Proc. Am. Soc. Testing Materials, 1957, v.57, pp. 751-755.
4. R. Pohlman, and B. Lehfeldt, “Influence of Ultrasonic Vibration on Metallic Friction”, Ultrasonics, 1966, pp. 178-185.
5. K. Siegert, “Influencing the friction in metal forming processes by superimposing ultrasonic waves”, CIRP Annals-Manufacturing Technology, 2001, v.50, n1, pp. 195-200.
6. M. Lucas, “Vibration sensitivity in the design of ultrasonic forming dies”, Ultrasonics, 1996, v.34, pp. 35-41.
7. V. P. Severdenko,V. Z. Zhilkin, “Wire drawing with ultrasound”, Russian Ultrasonics, 1974, v.4, n1, pp. 17-22.
8. V. P. Severdenko,V. S. Pashchenko, “Effect of die geometry on process of drawing with radial ultrasonic vibrations”, Izvestiya VUZ Chernaya Metallurgiya, 1978, pp.96-97.
9. K. Siegert, “Wire drawing with ultrasonically oscillating dies”, Journal of Materials Processing Technology, 1996, pp. 657-660.
10. M. Murakawa, “The utility of radially and ultrasonically vibrated dies in the wire drawing process”, Journal of Materials Processing Technology, 2001, pp. 81-86.
11. M. Hayashi, “Study on drawing using bisected dies vibrated ultrasonically and transversally”, Journal of the JSTP, 2001, v.42, pp. 1070-1074.
12. J. Tsujion, “Ultrasonic vibration bending of metal plate specimens”, Proc. IEEE 1989 Ultrasonic Symposium, 1990, pp. 1099-1102.
13. J. Tusjion, “Characteristics of ultrasonic bending of metal plates using a longitudinal vibration die and punch”, Proc. IEEE 1992 Ultrasonic Symposium, 1992, pp. 863-866.
14. T. Jimma, “An application of ultrasonic vibration to the deep drawing process”, Journal of Materials Processing Technology, 1998, pp. 406-412.
15. M. Jin, “Utility of ultrasonic vibration applied to metal-forming processes”, Advanced Technology of Plasticity, 1999, pp.19-24.
16. J. Petruzelka, “The effect of ultrasonic on tube drawing”, Journal of Materials Processing Technology, 1996, pp. 661-668.
17. M. Jin, “Fine-element simulation of ultrasonic wire drawing process”, Simulation of Materials Processing, 2001, pp. 475-479.
18. Z. Huang, M. Lucas, M. J. Adams, “Influence of ultrasonics on upsetting of a model paste”, Ultrasonics, 2002, v.40, pp. 43-48.
19. A. H. Cottrell, “Dislocations and plastic flow in crystals” Oxford at Clarendon Press, London, 1953.

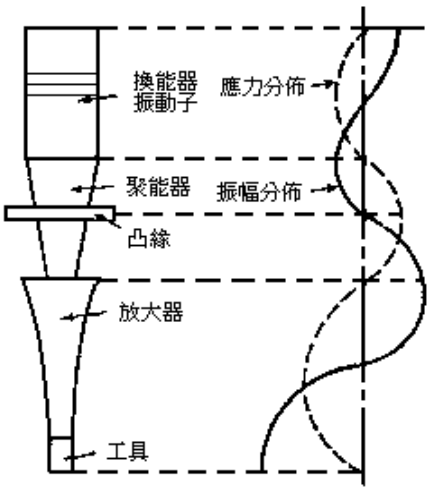

圖 1 超音波加工原理示意圖

圖 2 各種形狀的喇叭

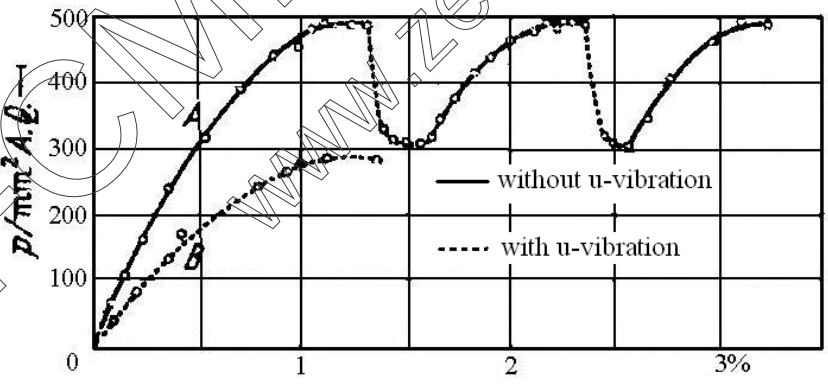

圖 3 超音波振動降低塑流應力比較圖【1】

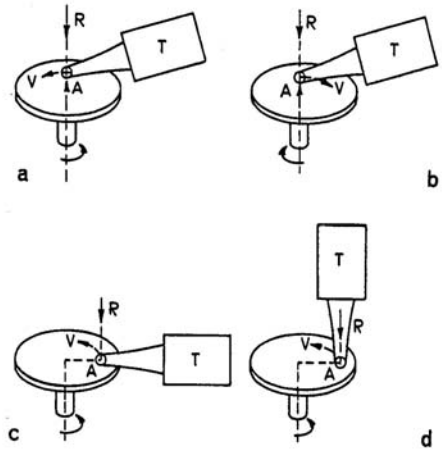

圖 4 振動方向降低摩擦力實驗裝置示意圖【4】

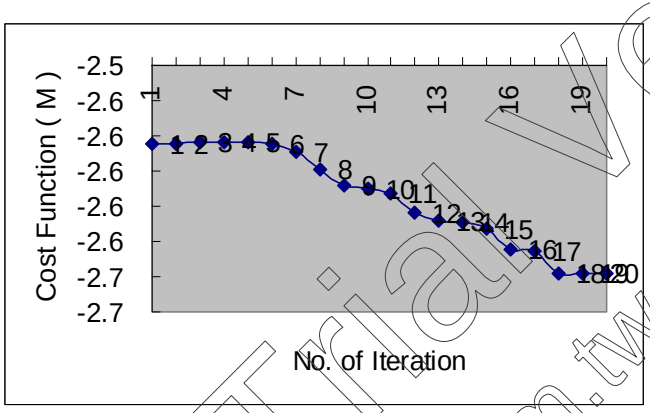

圖 5 階級形放大器之雙變數最佳化振幅放大因子收斂圖

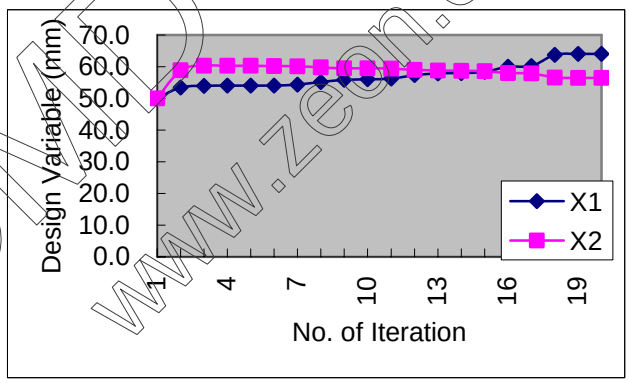

圖 6 階級形放大器之雙變數最佳化設計變數收斂圖

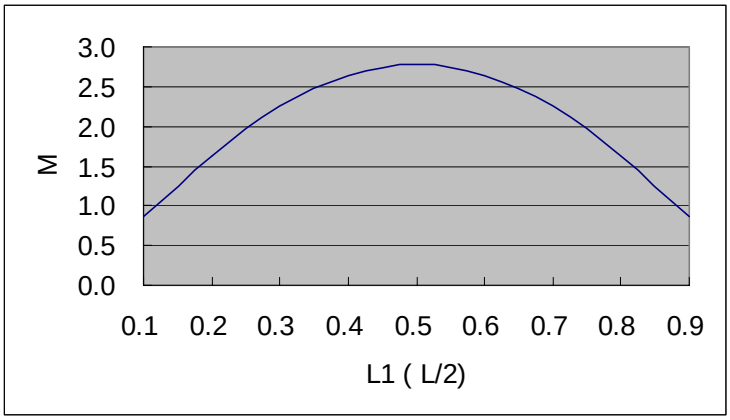

圖 7 階級形放大器理論近似解曲線

圖 8 超音波振動高溫壓縮實驗設備

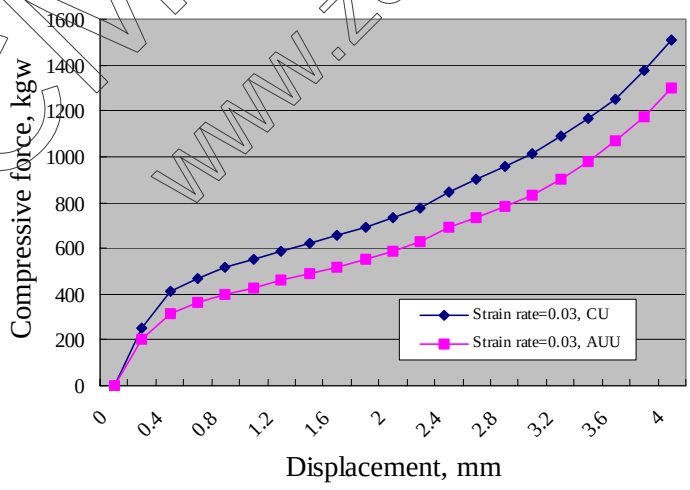

（a） T=25°C，CU 與 AUU 之負荷位移圖

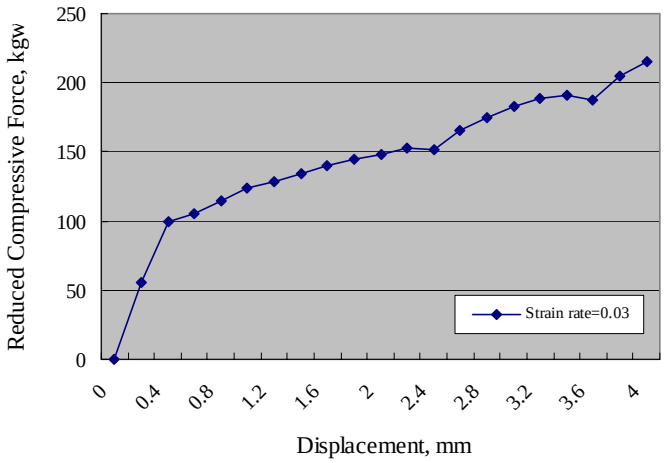

（b）T=25°C，降低變形阻力位移圖

圖 9 溫度 25°C， CU 與 AUU 之實驗結果圖

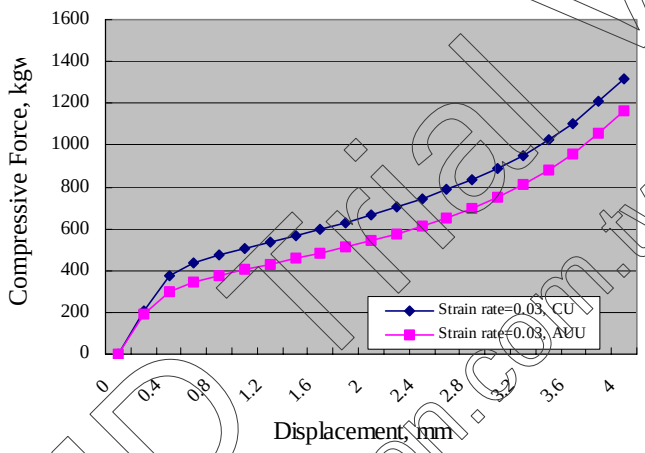

圖 10 溫度 100°C， CU 與 AUU 之負荷位移圖

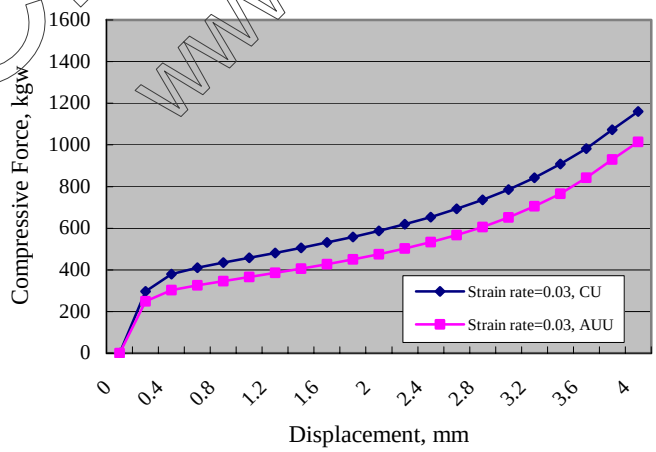

圖 11 溫度 200°C， CU 與 AUU 之負荷位移圖

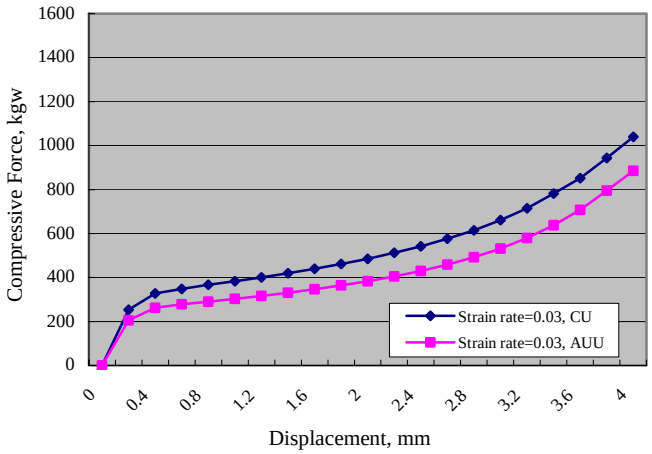

(a) T=250°C，CU 與 AUU 之負荷位移圖

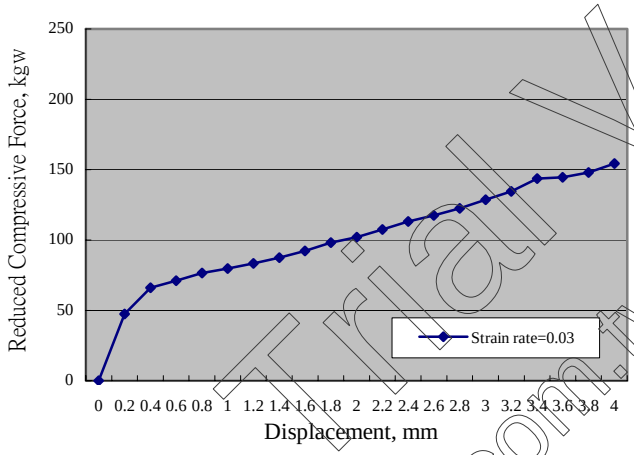

（b）T=250°C，降低變形阻力位移圖

圖 12 溫度 250°C， CU 與 AUU 之實驗結果圖

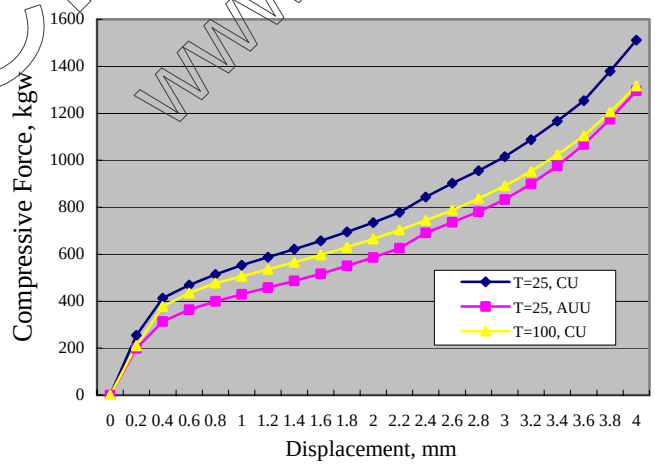

(a) T=25°C，CU 及 AUU 與 T=100°C 時 CU 之負荷位移比較圖

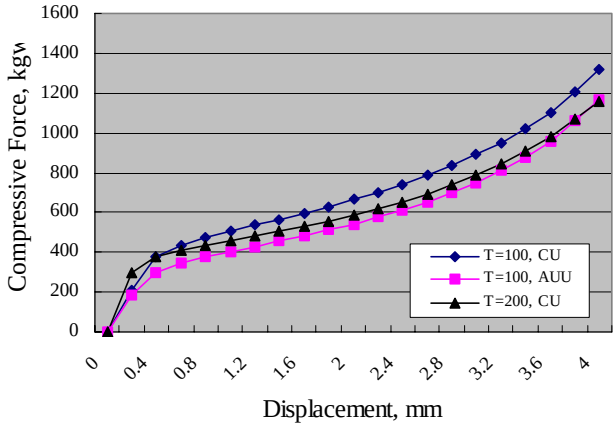

(b) T=100°C，CU 及 AUU 與 T=200°C 時 CU 之負荷位移比較圖

圖 13 CU 加熱與 AUU 實驗結果比較圖

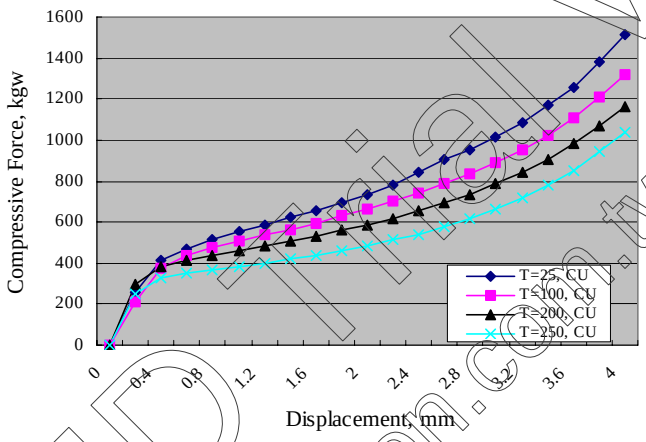

(a) CU 在各溫度之下負荷位移比較圖

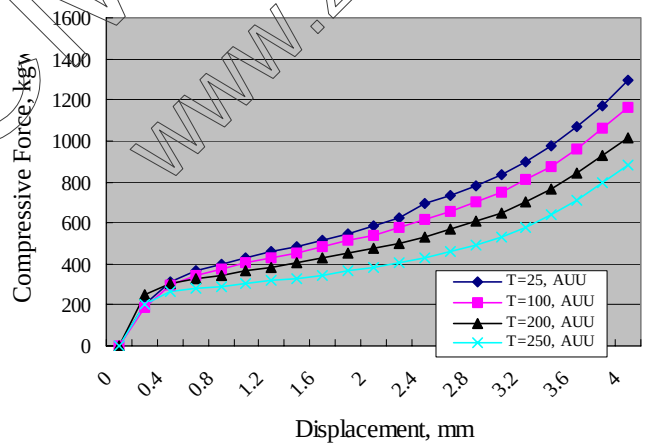

(b) AUU 在各溫度之下負荷位移比較圖

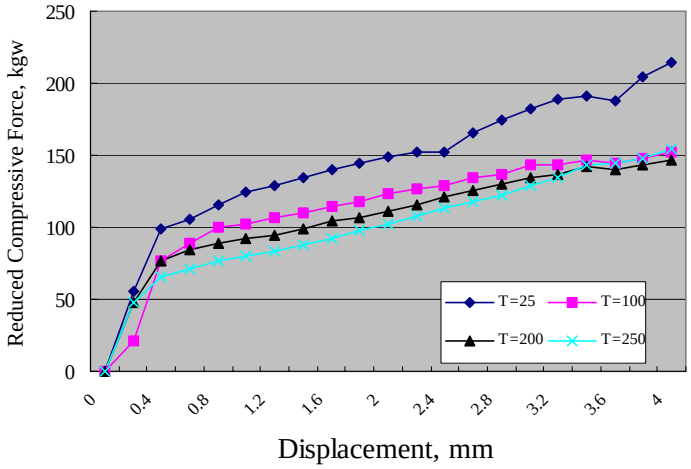

(c)各溫度超音波振動效應降低負荷位移比較圖

圖 14 各溫度下 CU 與 AUU 實驗結果比較圖

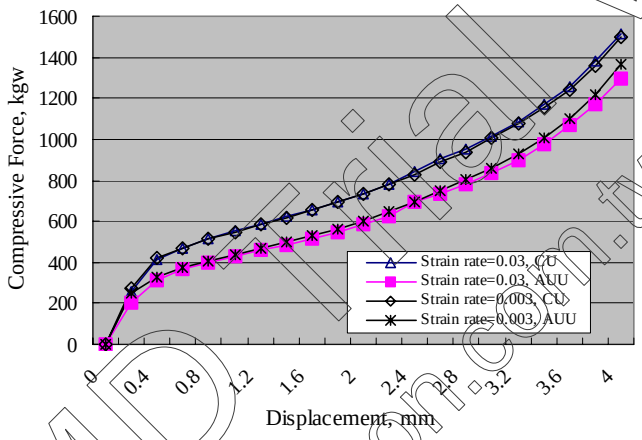

圖 15 溫度 25°C，不同速率下 CU 與 AUU 之實驗結果圖

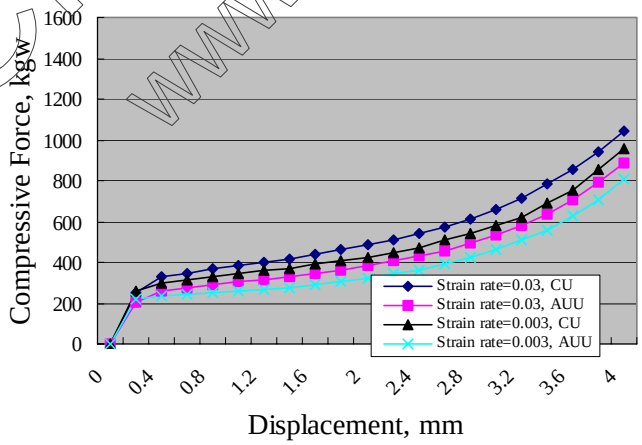

圖 16 溫度 250°C，不同速率 CU 與 AUU 之實驗結果圖

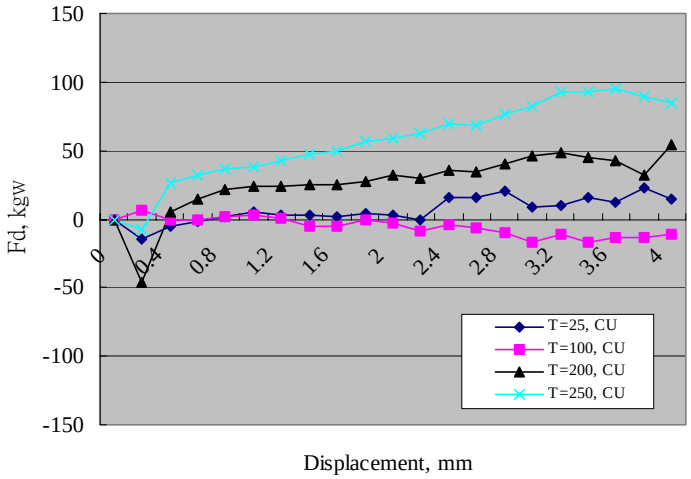

圖 17 CU 在不同速率，壓縮力相差值與位移比較圖

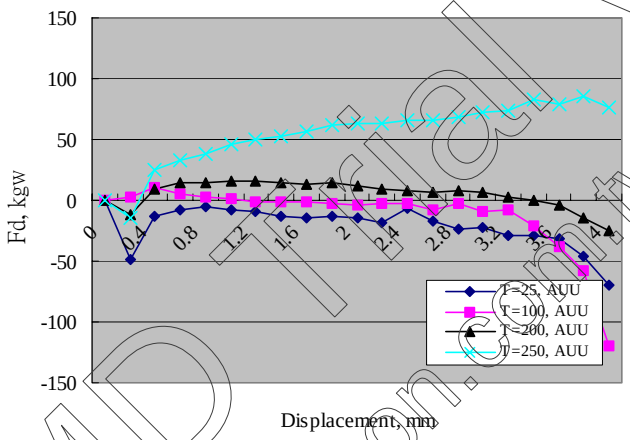

圖 18 AUU 之壓縮力相差值與位移比較圖

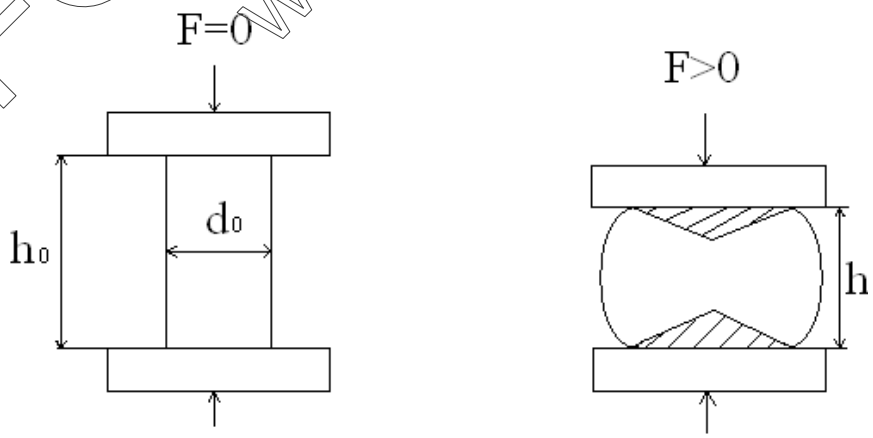

圖 19 單軸壓縮試驗產生桶狀外型示意圖

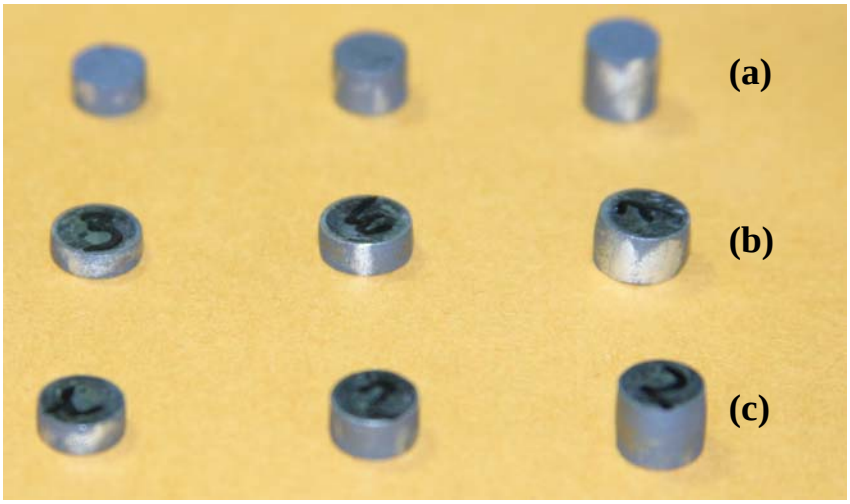

圖 20 修正單軸壓縮試驗試片實體圖，(a) 為壓縮試片實體 (b) 壓縮負荷為 1100kg 之超音波壓縮實驗結果 (c) 同負荷 1100kg 之無超音波壓縮實驗結果

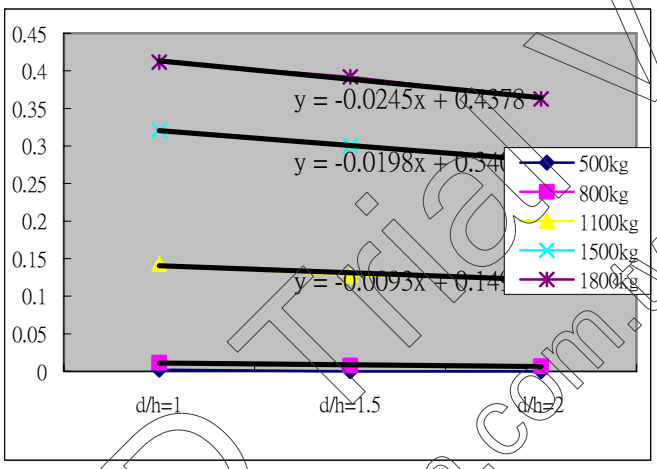

(a) 傳統單軸壓縮試驗之端點效應修正圖

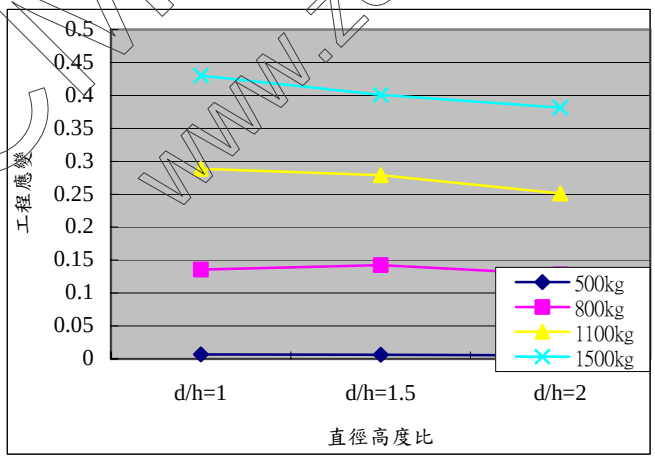

(b) 超音波振動單軸壓縮試驗之端點效應修正圖

圖 21 單軸壓縮試驗之端點效應修正圖

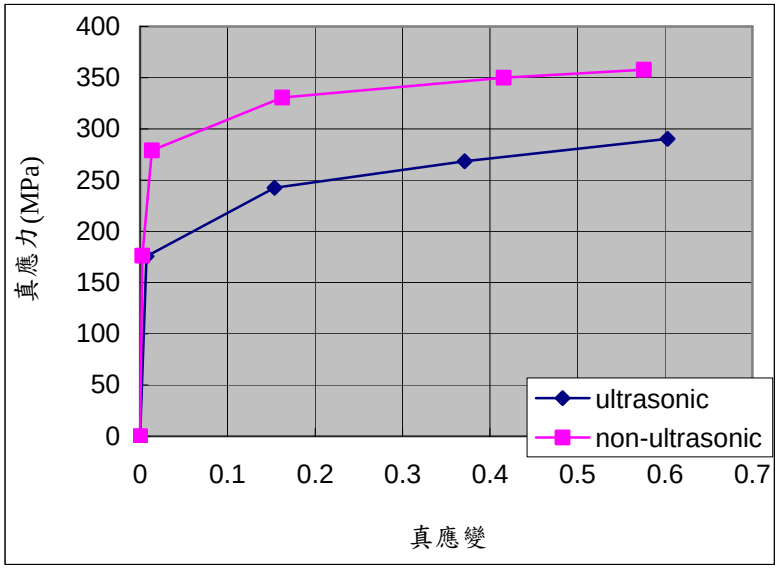

圖 22 傳統與超音波振動修正單軸壓縮實驗結果比較圖

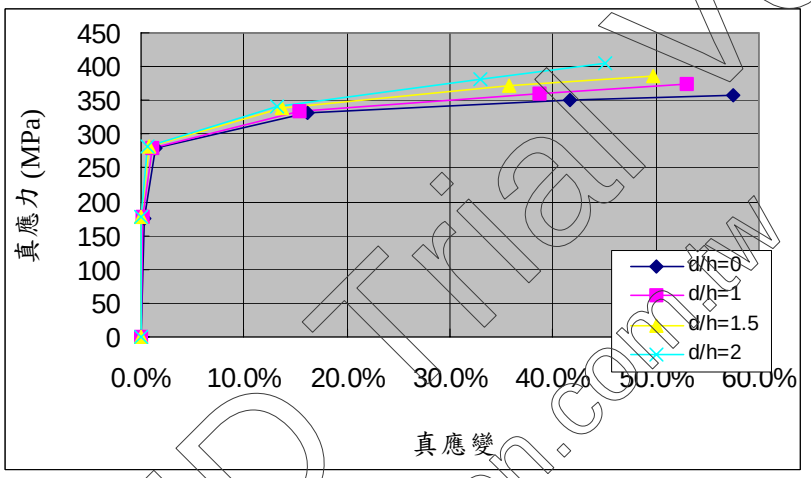

圖 23 傳統單軸壓縮不同直徑高度比之真應力-應變比較圖

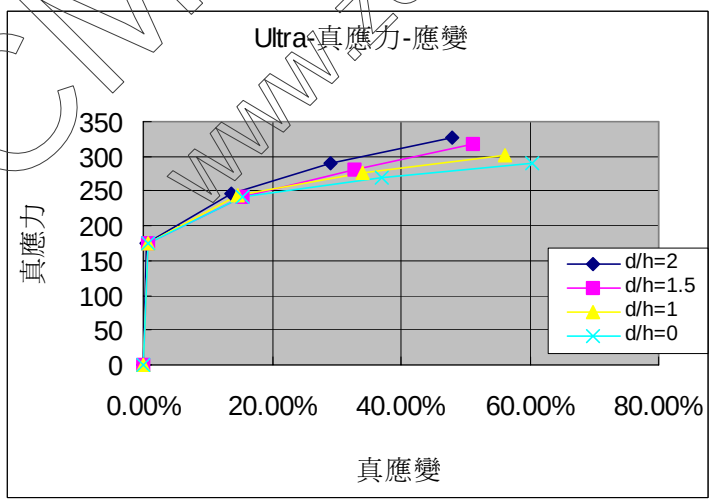

圖 24 超音波振動單軸壓縮不同直徑高度比之真應力-應變比較圖

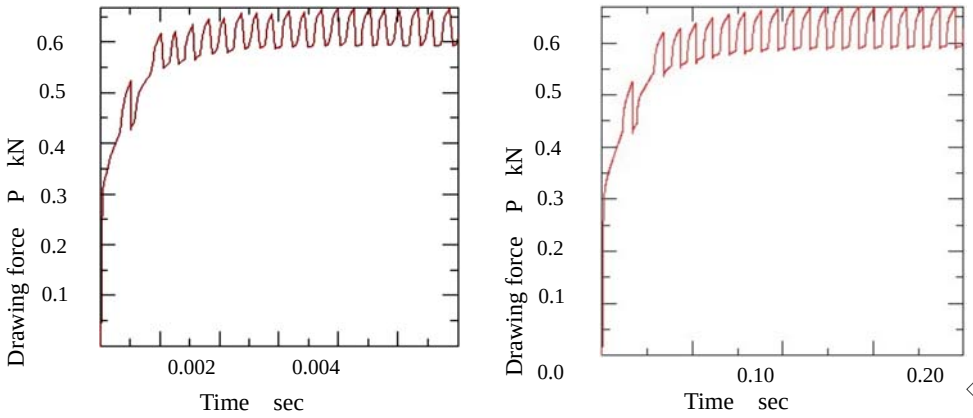

(a) V_d = 30 mm/s　　(b) V_d = 1000 mm/s

圖 25 有限元素模擬傳統抽拉（CD）之抽拉力結果圖（振幅 1μm）

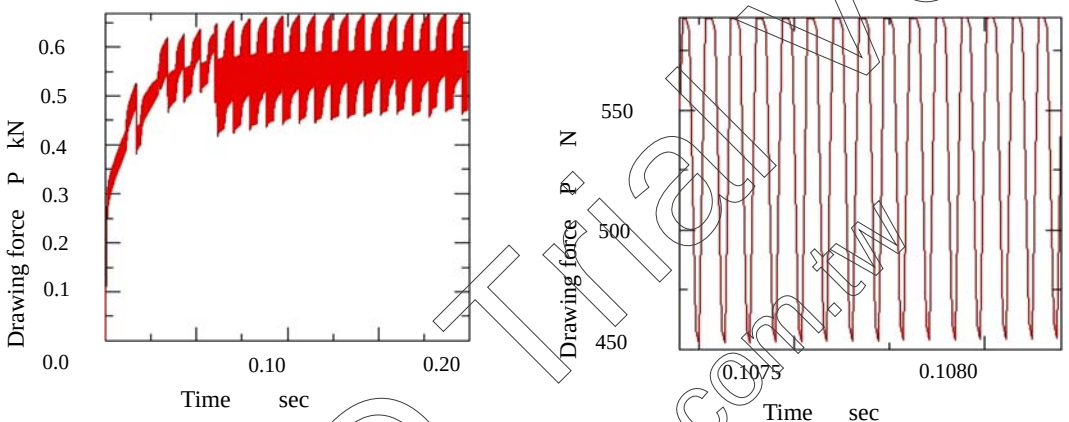

(a) V_d = 30 mm/s　　(b) Details of the fluctuation period for drawing force (V_d = 30 mm/s)

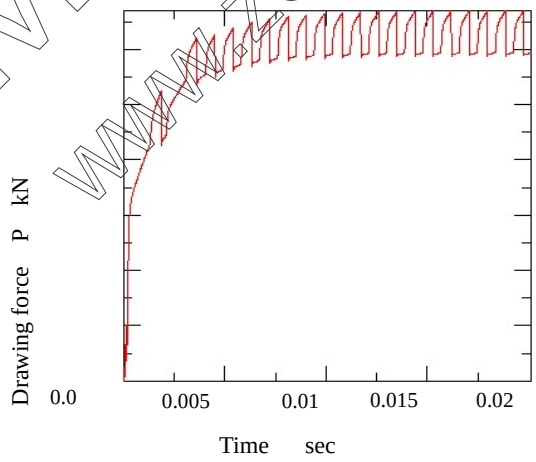

(c) V_d = 300 mm/s

圖 26 有限元素模擬軸向振動抽拉（AUD）之抽拉力結果圖（振幅 1μm）

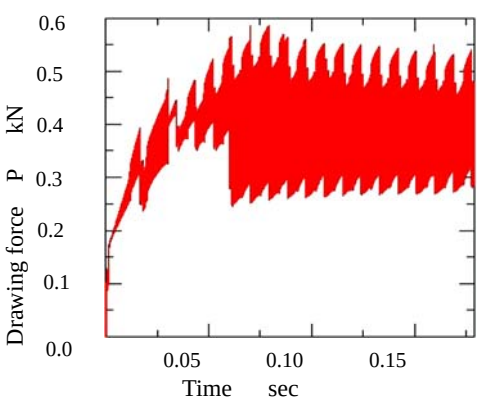

(a) V_d = 30 mm/s

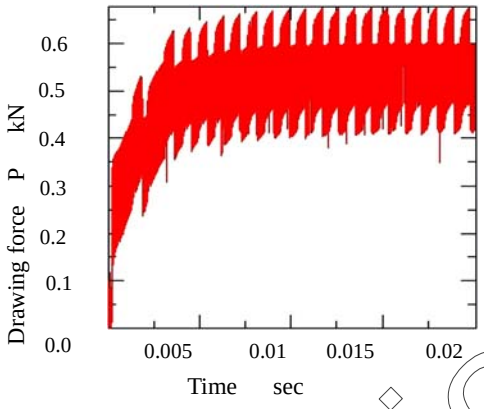

(b) Details of the fluctuation period for drawing force

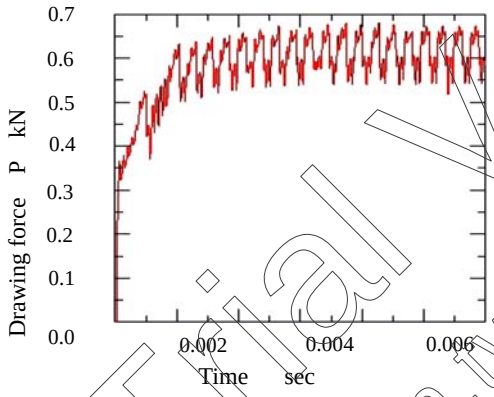

(c) V_d = 300 mm/s

圖 27 有限元素模擬軸向振動抽拉（AUD）之抽拉力結果圖（振幅 1μm）

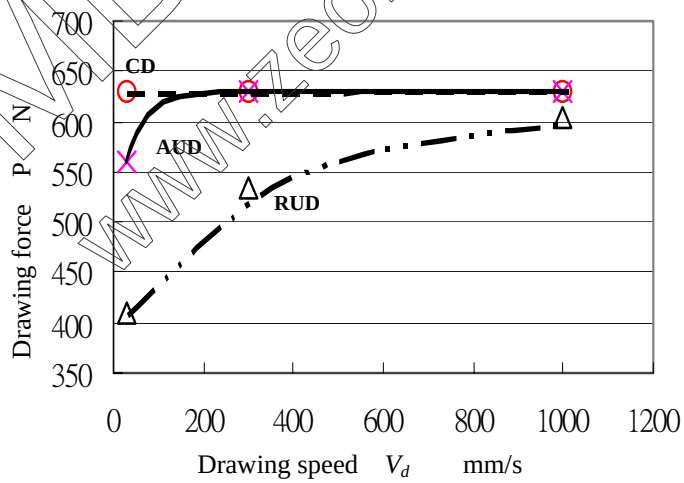

圖 28 有限元素模擬 CD、AUD 和 RUD 之抽拉速度與抽拉力關係圖

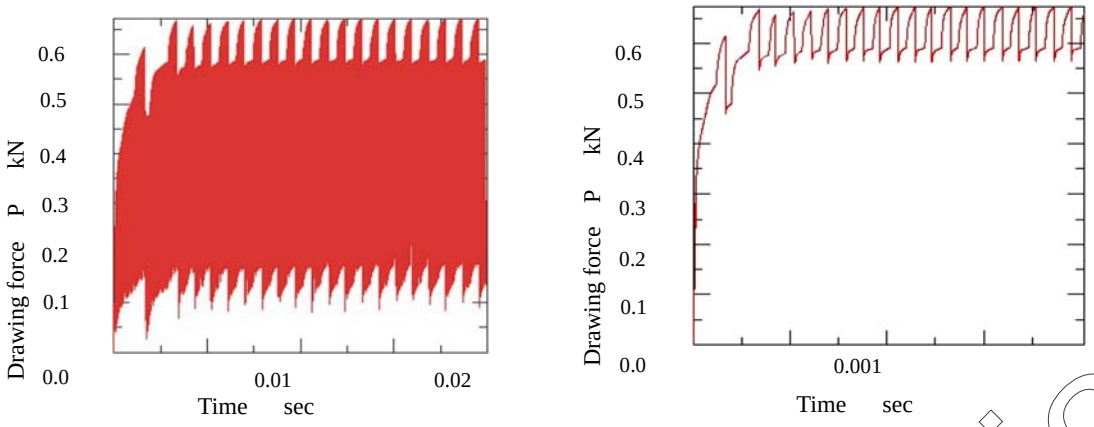

(a) V_d = 300 mm/s　　(b) V_d = 3000 mm/s

圖 29 AUD 不同抽拉速度之模擬分析抽拉力的結果圖（振幅 10 μm）

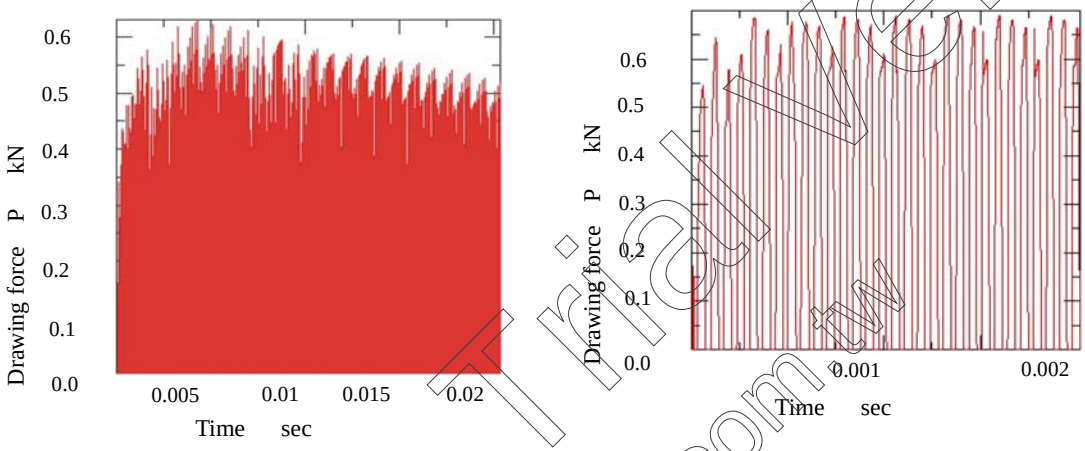

(a) V_d = 300 mm/s　　(b) V_d = 3000 mm/s

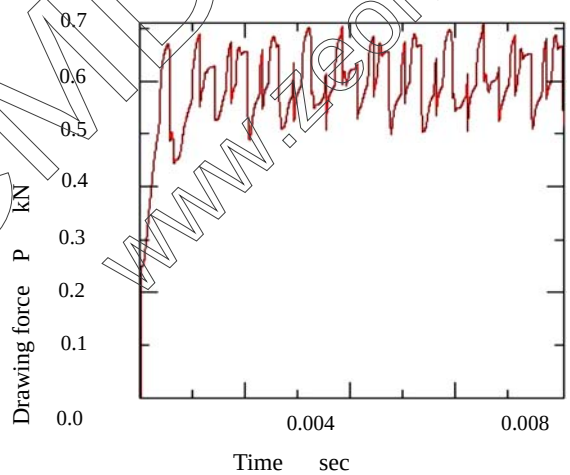

(c) V_d = 9000 mm/s

圖 30 AUD 不同抽拉速度之模擬分析抽拉力的結果圖（振幅 10 μm）

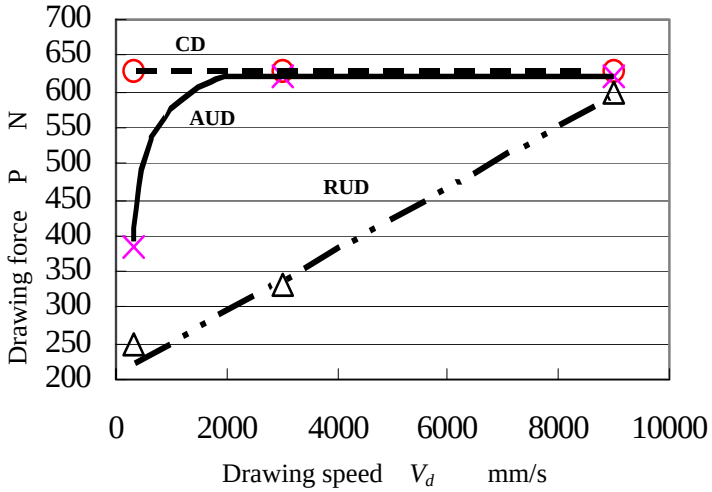

圖 31 CD、AUD 和 RUD 之抽拉速度與抽拉力模擬結果關係圖（振幅 10 μm）

8. 計畫成果自評

雖然本研究計畫原本預計針對超音波輔助複合擠製成形進行研究，前兩年為基礎、特性研究，第三年為擠製之應用。但是，由於擠製成形製程於成形時所需之工作應力相當大，受限於現階段尚無法取得高輸出功率，且可長時間運作之超音波振動設備。因此本研究前兩年將針對超音波振動高溫壓縮、衝壓進行研究，探討超音波振動作用於成形時，所產生一些現象。並將這些基礎研究所得，於第三年投入成形所需功率較低的應用項目上，陸續完成了超音波輔助鋁線抽拉（與日本工業大學進行之國際學術合作，由本實驗室負責有限元素之模擬分析）及鋁合金端面熱壓的研究，並發表於國際期刊上。

由整個計畫執行過程中，於每個計畫執行階段，計畫執行所預期之目標均已完成，而整個研究過程中所執行之目標與成果敘述如下：

實驗設備製作方面：

1. 證實超音波振動系統於高溫環境下運作之可行性。
2. 高溫端面壓縮實驗中，爐內溫度與試片溫度相差甚大，必須於模具設計加熱裝置，進行溫度補償。
3. 建立完成高溫環境下超音波振動成形之實驗裝置。

數值模擬分析與最佳化：

2. 證實超音波振動系統於高溫環境下運作之可行性。
3. 實驗證明，研究中所建立之有限元素分析模型能縮短振幅放大器設計製作時間，且有效預測共振頻率與振幅分佈。
4. 建立完成有限元素模擬分析與最佳化系統之整合技術，提供一精準快速且自動化之振幅放大器最佳化設計系統。
5. 由有限元素分析與最佳化系統整合所得之最佳解，較理論近似解更接近實驗值。

超音波振動於鋁合金高溫端面壓縮實驗：

1. 證實超音波振動系統於高溫環境下運作之可行性。
2. 實驗證明，軸向超音波振動能有效降低高溫端面壓縮時成形力量。
3. 高溫端面壓縮實驗中，超音波振動使成形力量降低的機制，由應力重疊、差排吸收超音波能量與介面摩擦力降低交互作用產生，非由單一效應所造成。
4. 超音波振動降低高溫端面壓縮時的成形力量，隨溫度升高而減少。
5. 應變速率對超音波振動降低材料塑流應力效應影響不大。

超音波振動於端面壓縮之摩擦影響：

1. 實驗證明，在無摩擦力影響之效應下，超音波振動作用，仍能有效降低材料塑性變形應力。
2. 超音波振動端面壓縮中，對於改善端面摩擦影響的效應很小。
3. 超音波振動端面壓縮成形時，超音波振動使成形力量降低的機制中，降低摩擦力效應的影響很小，故此效應可排除。

超音波振動線材抽拉之有限元素模擬分析：

1. 建立一個徑向超音波抽拉與軸向超音波抽拉時，抽拉力波形之定量分析方法，證明抽拉力波形隨著超音波振動的週期而改變。

2. 由 FEM 分析所得到的臨界抽拉速度與理論值想當一致，且與實驗結果得到的抽拉速度相的符合。
3. AUD 和 RUD 之抽拉力波形變動的頻率平均值與實驗抽拉力量測結果非常一致。
4. 由有限元素的定量分析驗證抽拉速度隨振幅減少而降低。

本研究目前已發表兩篇國際期刊及兩篇會議論文（如附錄）：

1. Masahiro Hayashi and Jung-Chung Hung, “Simulation of Ultrasonic-Vibration Drawing Using the Finite Element Method (FEM)”, Journal of Materials Processing Technology, 2003, Vol. 140, pp. 30-35
2. Jung-Chung Hung, Chinghua Hung “The influence of ultrasonic-vibration on hot upsetting of aluminum alloy”, Ultrasonics, 2005, Vol. 43, pp. 692-698

研討會論文

1. Masahiro Hayashi and Jung-Chung Hung, 2003, “Simulation of Ultrasonic-Vibration Drawing Using the Finite Element Method (FEM)”, 6th Asia Pacific Conference on Materials Processing, Taipei, Taiwan.
2. 洪榮崇, 洪景華, 2004, “超音波振動於鋁合金高溫壓縮之影響”,中國工程師學會第二十一屆全國學術研討會。

附　錄

國際期刊:

1. Masahiro Hayashi and Jung-Chung Hung, “Simulation of Ultrasonic-Vibration Drawing Using the Finite Element Method (FEM)”, Journal of Materials Processing Technology, 2003, Vol. 140, pp. 30-35
2. Jung-Chung Hung, Chinghua Hung “The influence of ultrasonic-vibration on hot upsetting of aluminum alloy”, Ultrasonics, 2005, Vol. 43, pp. 692-698

研討會論文:

1. Masahiro Hayashi and Jung-Chung Hung, 2003, “Simulation of Ultrasonic-Vibration Drawing Using the Finite Element Method (FEM)”, 6th Asia Pacific Conference on Materials Processing, Taipei, Taiwan.
2. 洪榮崇, 洪景華, 2004, “超音波振動於鋁合金高溫壓縮之影響”,中國工程師學會第二十一屆全國學術研討會。

Available online at www.sciencedirect.com
SCIENCE DIRECT®
Ultrasonics 43 (2005) 692–698
Ultrasonics
www.elsevier.com/locate/ultras

The influence of ultrasonic-vibration on hot upsetting of aluminum alloy

Jung-Chung Hung, Chinghua Hung *

Department of Mechanical Engineering, National Chiao Tung University, 1001 Ta Hsueh Road, Hsinchu 300 Taiwan, ROC

Received 2 November 2004; received in revised form 2 March 2005; accepted 8 March 2005
Available online 23 March 2005

Abstract

The traditional ultrasonic apparatus cannot be operated at high temperature, explaining why the effect of ultrasonic-vibration on high temperature metal forming has seldom been addressed in literature. This study establishes an ultrasonic-vibration hot upsetting system. A cooling mechanism is used to solve the problem of high temperature. The effects of temperature and strain rate during ultrasonic-vibration on the upsetting of aluminum alloy were explored using this new system. Experimental results indicate that ultrasonic-vibration can considerably reduces the compressive forces during hot upsetting. The reducing effect on compressive forces decreases while the temperature increases. The strain rate does not significantly affect the reducing effect on compressive forces.

Keywords: Ultrasonic-vibration; Hot upsetting; Aluminum alloy

1. Introduction

Many new materials, such as titanium alloys, magnesium alloys and inter-metallic compounds, are difficult to produce. Production depends on the development of new processes to overcome the difficulties that arise during the metal forming process. The technique of ultrasonic-vibration has been applied widely in metal forming. The difference between conventional metal forming and the ultrasonic-vibration metal forming is that the latter exploits ultrasonic energy to act on the die and then uses the die to deform the work-piece.

Some interesting effects arise in the application of ultrasonic-vibration for metal forming processes, such as the reduction of the friction between the die and the work-piece, the reduction of the forming forces, and decreases of the spring-back angle during sheet metal forming. These effects increase the forming limit of materials. Blaha and Langenecker were the first to investigate the use of ultrasonic-vibration in relation to plasticity of metals [1,2]. They superimposed high-frequency vibrations onto the static load during the tensile testing of a zinc single crystal specimen. In the experiment, they observed a substantial reduction in the yield stress and the reduction of the flow stress. This phenomenon is the so-called Blaha effect. Kempe [3] proposed three mechanisms by which dislocations may absorb energy from vibrations; they are (1) a resonance mechanism, (2) a relaxation mechanism, and (3) a mechanism of simple hysteresis. Nevill [4] attributed the reduction of the flow stress to the superposition of steady stress and the alternation of stress, and proposed the stress superposition mechanism.

Lehfeldt and Pohlman [5] examined the feasibility of exciting a ball by vibration on a revolving plate in experiments on the influence of the ultrasonic-vibration on friction. The frictional forces are minimal at the contact surface when the direction of vibration is parallel to the direction of motion. Jimma et al. [6] applied ultrasonic-vibration to the deep drawing process and show that

* Corresponding author. Tel.: +886 3 5712121 55160; fax: +886 3 5720634.
E-mail address: chhung@mail.nctu.edu.tw (C. Hung).

0041-624X/$ - see front matter © 2005 Elsevier B.V. All rights reserved.
doi:10.1016/j.ultras.2005.03.001

ultrasonic-vibration deep drawing is very effective in increasing the limiting drawing ratio (LDR) and surpassed the theoretical value LDR of deep drawing by ideal tools without friction. Murakawa et al. [7,8] investigated the effects of radial ultrasonic-vibration drawing (RVD) and axial ultrasonic-vibration drawing (AVD), and compared them to those of conventional wire drawing (CD). It was proven to be highly effective in increasing the critical drawing speed by ultrasonic wire drawing, and the RVD operation appears to be more productive than the AVD operation.

Huang et al. [9] investigated the benefits of applying the axial ultrasonic-vibration of forming tools in an upsetting process; he used plasticine as a model material to simulate the hot metal. According to that study, applying an ultrasonic-vibration to the die reduces the mean forming force during upsetting. He concluded that the stress superposition effect and the reduction of interface friction contributed to the above phenomenon.

Conventional ultrasonic apparatus cannot be operated at high temperatures, so relatively few investigations have addressed the effect of ultrasonic-vibration metal forming at high temperature. This study, establishes an ultrasonic-vibration hot upsetting apparatus to overcome this difficulty. The effects of temperature and strain rate during ultrasonic-vibration on the hot upsetting of aluminum alloy are investigated using this apparatus.

2. Ultrasonic-vibration hot upsetting apparatus

2.1. Hot upsetting machine

Hot upsetting is based on a process of unconfined uni-axial deformation of a cylindrical specimen between parallel rigid platens. In this study, an especially designed microcomputer server controls the hot upsetting machine. The machine has four conducting pillars and a server motor to control the velocity of the platens. The maximum loading capacity is 2000 kg W; resolution of the force is 10 N; the resolution of displacement is 0.005 mm and the range of velocity is 0.5–50 mm/min. Fig. 1 shows this machine.

2.2. Heating and cooling system

Materials are easily oxidized at high temperature, so the heating system is enclosed in a vacuum chamber, which can sustain a maximum temperature of 600 °C and vacuum pressure of 10^{-3} Torr. The system was designed with a free moveable die and a vacuum furnace and so was ideal for performing experiments at a high temperature in a vacuum.

During the ultrasonic-vibration hot upsetting experiment, heat may be transferred to the mechanical apparatus affecting the parts. The vacuum furnace and the both upper and lower dies also require a cooling system to prevent damage to the part. The heating of the dies proceeds mainly by thermal radiation, so the rate of heating was lower than the rate of liquid cooling. An auxiliary heating system was designed on both the upper and lower dies to make compensate for the heat to increase the accuracy of the temperature control. Three independent PID controlled are used to control the temperature. This temperature compensation can maintains the temperature between the dies and the inner furnace within ±1 °C.

Fig. 1. Ultrasonic hot upsetting experiment set up.

2.3. Ultrasonic-vibration system

The ultrasonic-vibration system includes an ultrasonic frequency generator, a piezoceramic vibration transducer, a resonator and an ultrasonic forming die. The ultrasonic frequency generator has a maximum capacity of 2 kW and provides power for a piezoelectric transducer to generate ultrasonic-vibration. This generator includes an automatic frequency-tracking controller, which is able to maintain the system resonant frequency at 20 kHz ± 300 Hz. A booster then amplifies the amplitude of vibration and transmits it to a horn. The ultrasonic-vibration system was fixed by flange located at the booster's vibration node. The step horn,

which is resonant in a longitudinal mode, was uniquely designed for use in upsetting. In this investigation, finite element simulations software, ABAQUS, was used to determine the dimensions of this stainless steel horn. The results of the tests showed that the simulated and experimental resonant frequencies were very close to each other.

3. Ultrasonic-vibration hot upsetting experiment

3.1. Experimental procedure

The ultrasonic-vibration hot upsetting experiment proceeded as follows. First, the ultrasonic-vibration system and vacuum furnace were set up on a hot bench controlled by a microcomputer server. Second, the specimen was placed between parallel dies. Then, a 20 kg W preload was applied to the specimen. The heating controller was turned on. When the temperature reached the designated temperature, it was hold constant for 10 min before the rest of the experiment was performed. Whenever the loading reached 70 kg W during an experiment, the ultrasonic-vibration was superimposed.

3.2. Experimental conditions

Table 1 shows material properties and the hot upsetting conditions used in the experiment. The specimens used in this study were aluminum alloy A6061 that was 6 mm high and 6 mm in diameter. The compression displacement was set to 4 mm (equivalent to a 66.7% compression ratio), and the true strain rate was controlled throughout the experiment. The tests were performed under dry conditions without lubricant. During ultrasonic-vibration hot upsetting, the axial vibration frequency was 20 kHz. The amplitude was set to 5.6 μm.

4. Experimental results and discussion

4.1. Effects of ultrasonic-vibration and temperature on upsetting

Fig. 2 shows the experimental results of load–displacement curves for the conventional upsetting (CU) and axial ultrasonic-vibration upsetting (AUU). The temperature was set to 25 °C and the true strain rate was 0.03 1/s. Fig. 2(a) shows that for CU, the compression ratio was 67% (with a displacement of 4 mm) under a compressive forces 1511 kg W for CU, but for AUU, a compressive forces was 1296 kg W was required to yield the same compression ratio. The compressive force was therefore 215 kg W lower for AUU. These results indicate that ultrasonic-vibration effectively reduces the material flow stress. Fig. 2(b) shows reduced compressive forces–displacement curves. Under ultrasonic-vibration, increasing the compression ratio increases the reduction in the compressive forces. Restated, ultrasonic-vibration strengthens the effect of the reduced compressive forces when the compressing ratio is increased.

Figs. 3–5 show the load–displacements curves of the CU and AUU, with a constant true strain rate of 0.03 1/s at temperatures set to 100 °C, 200 °C and 250 °C, respectively. At all tested temperatures, the load decreased when the ultrasonic-vibration was applied.

Fig. 6(a) and (b) plot the relationship between temperature and ultrasonic-vibration. When the compression

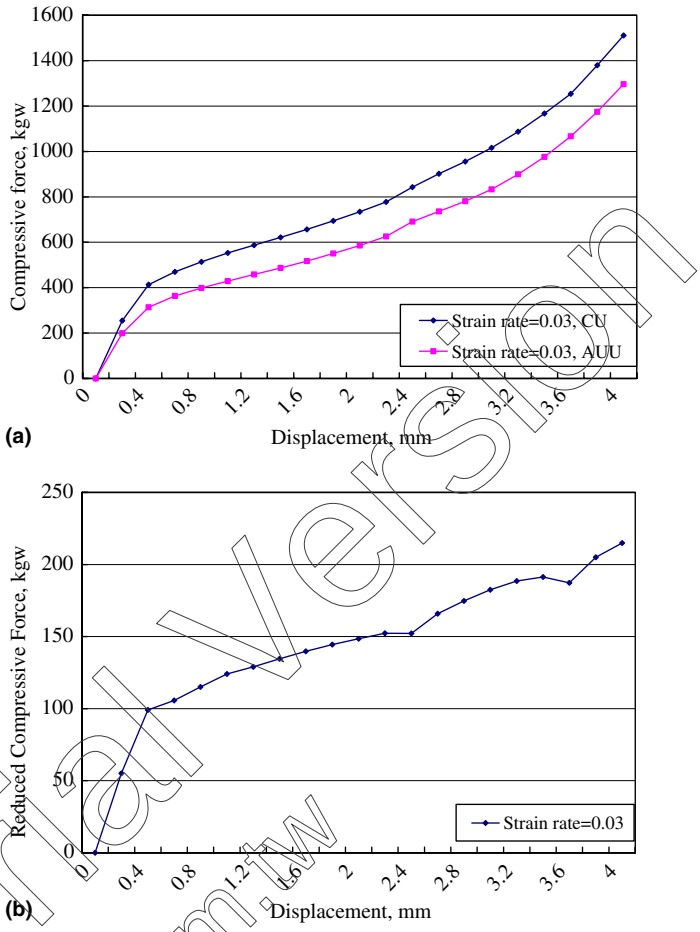

Fig. 2. Load–displacement curves for CU and AUU at 25 °C: (a) compressive forces–displacement curves for CU and AUU; (b) reduced compressive forces–displacement curves.

Table 1
Material and hot upsetting conditions

Specimen material	Aluminum alloy (A 6061)
Tooling material	Stainless steel (SUS304)
Size of specimen	$\phi 6.0 \times 6.0$ mm
Lubricant	N/A
Reduction (R)	66.7%
True strain rate ($\dot{\varepsilon}$)	0.003 1/s, 0.03 1/s
Temperature of specimen	25 °C, 100 °C, 200 °C, 250 °C

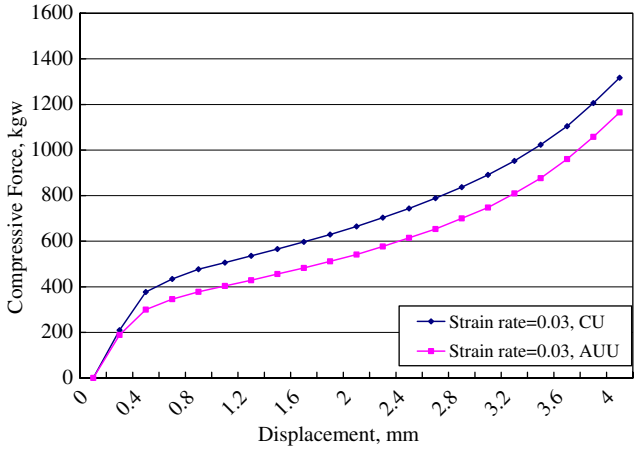

Fig. 3. Load–displacement curves for CU and AUU at 100 °C.

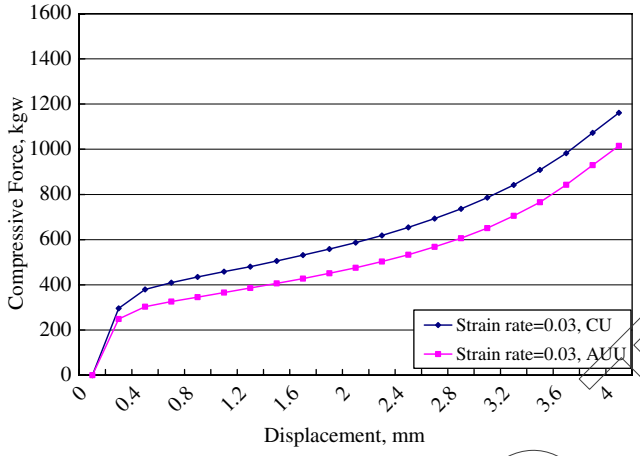

Fig. 4. Load–displacement curves for CU and AUU at 200 °C.

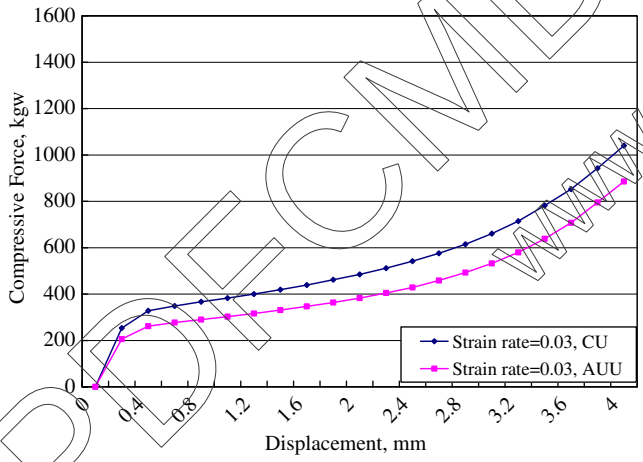

Fig. 5. Load–displacement curves for CU and AUU at 250 °C.

displacement was 4 mm the compressive forces of AUU at 25 °C and 100 °C were very close to those of CU at 100 °C and 200 °C. Accordingly, the reduction in flow stress caused by increasing the temperature by 100 °C is comparable to that caused by applying ultrasonic-

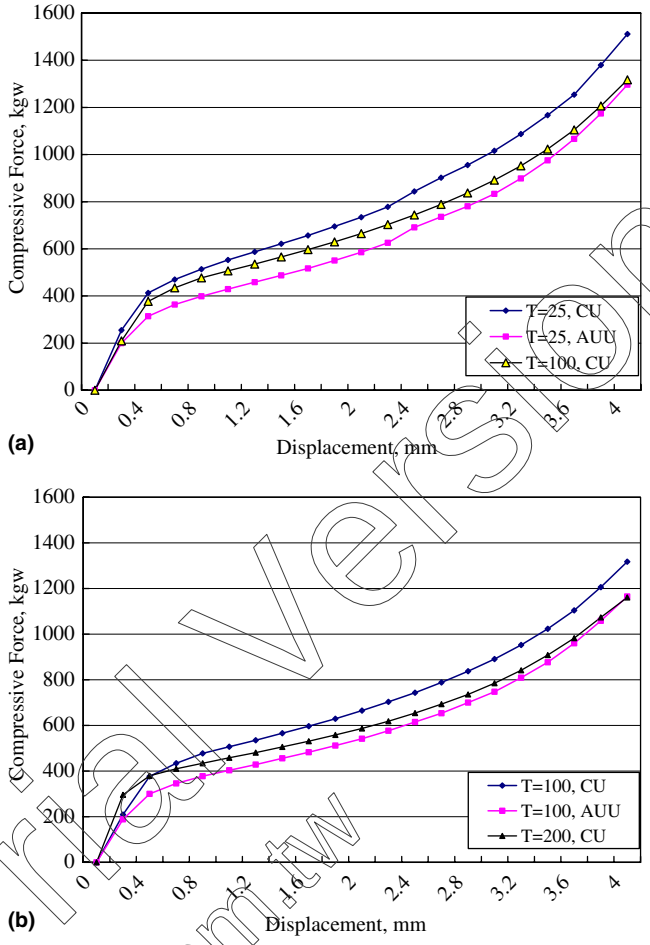

Fig. 6. Relationship between temperature and ultrasonic-vibration in CU and AUU: (a) load–displacement curves of CU at 25 °C and 100 °C, AUU at 25 °C; (b) load–displacement curves of CU at 100 °C and 200 °C, AUU at 100 °C.

vibration. However, when the compression displacement was less than 3 mm, the effect of ultrasonic-vibration exceeded than that of increasing the temperature by 100 °C.

Fig. 7(a) and (b) indicate that the increase in temperature reduced compressive forces for CU and AUU at a true strain rate of 0.03 1/s. Fig. 7(c) plots the load–displacement curve of the compressive forces reduced by ultrasonic-vibration at various temperatures. The reduction in compressive forces caused by ultrasonic-vibration was distinguished at 25 °C. The magnitude of the compressive forces reduction caused by ultrasonic-vibration decreases as the temperature is increased.

4.2. Effects of ultrasonic-vibration and strain rate on upsetting

In this part, the true strain rate was set to 0.03 1/s and 0.003 1/s in CU and AUU, respectively, at temperatures from 25 °C to 250 °C. Fig. 8 shows that the strain rate did not influence CU and AUU at 25 °C. In Fig. 9, when

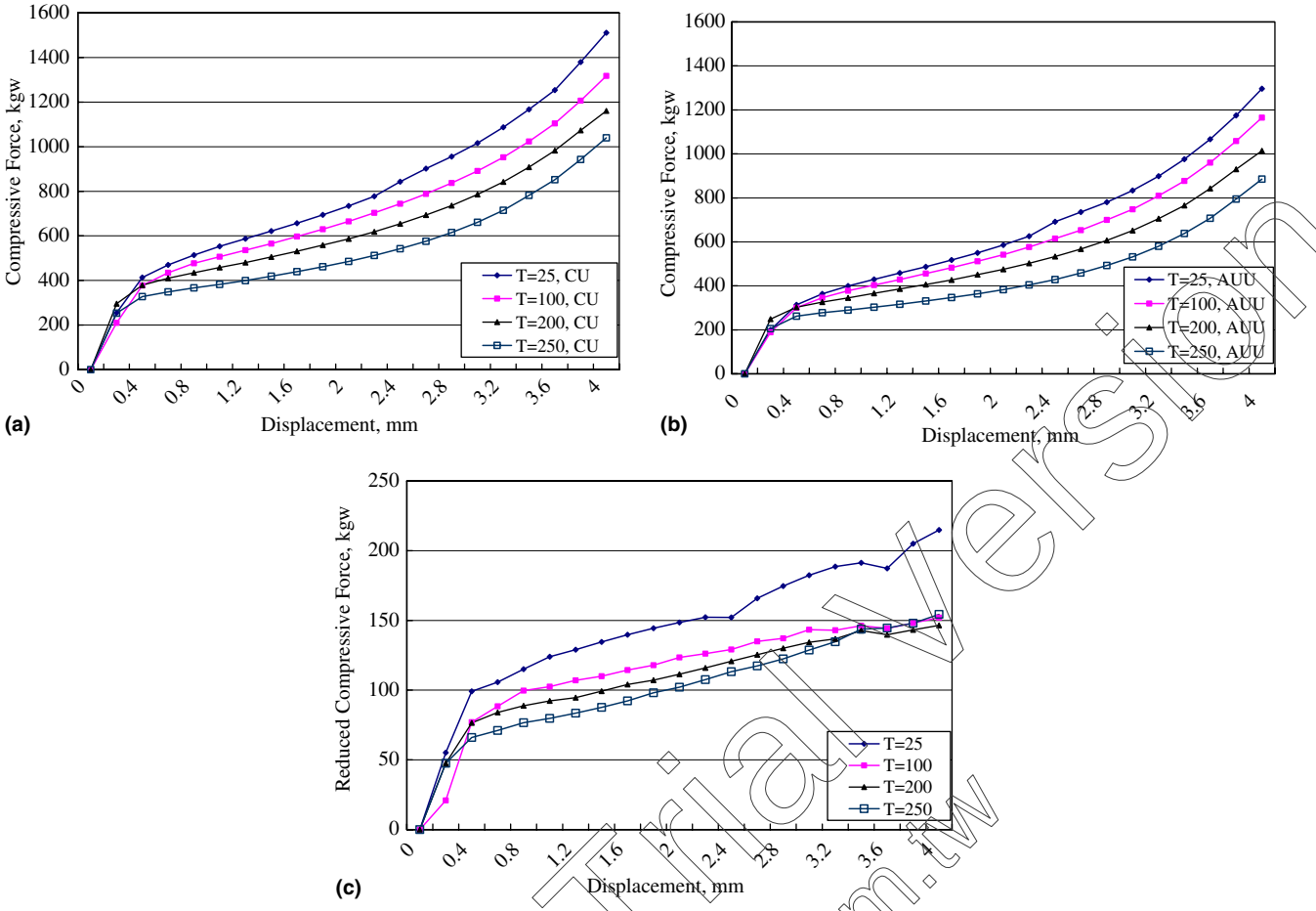

Fig. 7. Experimental results for CU and AUU at 25 °C, 100 °C, 200 °C and 250 °C: (a) load–displacement curves of CU at 25 °C, 100 °C, 200 °C and 250 °C; (b) load–displacement curves of AUU at 25 °C, 100 °C, 200 °C and 250 °C; (c) reduced force-displacement curves for AUU at 25 °C, 100 °C, 200 °C and 250 °C.

the temperature was increased to 250 °C, the loading force of CU and AUU decreased as the strain rate was lowered to 0.003 1/s. These results indicated that, at high temperature, the strain rate markedly affected the material's flow stress, regardless of whether ultrasonic-vibration was applied.

Fig. 10 shows the differences of compressive forces vs. displacements of CU at true strain rates of 0.03 1/s and 0.003 1/s. The difference of compressive forces (F_d) is defined as

$$F_d = F_{\dot{\varepsilon}=0.03} - F_{\dot{\varepsilon}=0.003} \quad (1)$$

where $F_{\dot{\varepsilon}=0.03}$ is the loading associated with a strain rate of 0.03 1/s and $F_{\dot{\varepsilon}=0.003}$ is the loading associated with a strain rate of 0.003 1/s.

Fig. 11 plots the differences of compressive forces vs. displacements of AUU at strain rates of 0.03 1/s and 0.003 1/s. At 250 °C for both CU and AUU, the strain rate significantly affects the compressive forces. Furthermore, when the displacement exceeded 3 mm in 25 °C and 100 °C, the difference of compressive forces becomes negative because the ultrasonic-vibration operation proceeds for a long time, increasing the system's temperature, reducing the efficiency of the power transformation of the system.

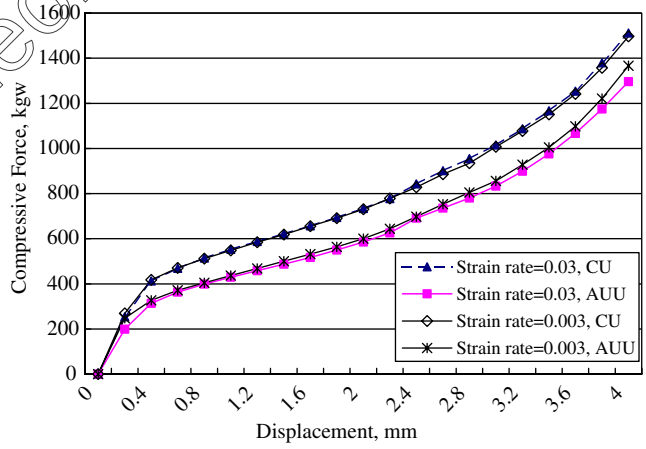

Fig. 8. Load–displacement curves for CU and AUU at 25 °C; the strain rate was 0.03 1/s and 0.003 1/s.

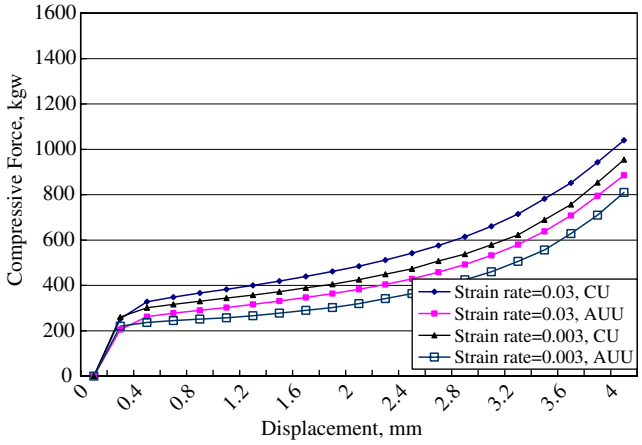

Fig. 9. Load–displacement curves for CU and AUU at 250 °C; the strain rate was 0.03 1/s and 0.003 1/s.

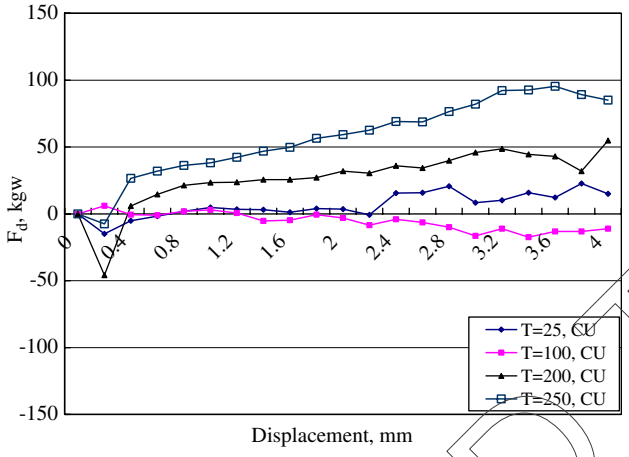

Fig. 10. Differences of compressive forces vs. displacements of CU in strain rate of 0.03 1/s and 0.003 1/s.

4.3. Mechanisms of ultrasonic-vibration in upsetting

Several investigations have demonstrated that the mechanisms of ultrasonic-vibration in metal forming are as follows: (1) reduction of flow stress; (2) reduction of the friction between die and work-piece, and (3) increase of the temperature between die and work-piece. The most common causes of the reductions of flow stress are as follows: (1) dislocations might absorb energy through resonance and overcome slip obstacles; (2) dislocations are able to absorb energy from an applied periodic stress and overcome the energy barrier; (3) the internal friction effect; and (4) the superposition of steady stress and alternating stress. Overall, the effects of ultrasonic-vibration on metal forming are very complex. Apart from the reduction of flow stress, the friction between die and work-piece and the raised temperature of the material must also be considered. For example,

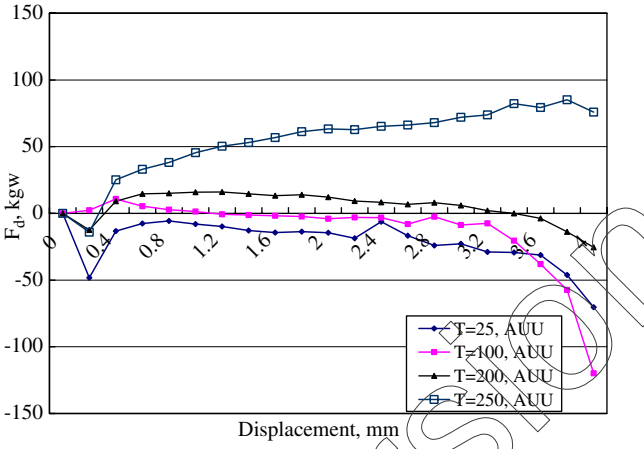

Fig. 11. Differences of compressive forces vs. displacements of AUU in strain rate of 0.03 1/s and 0.003 1/s.

the friction effect is stronger when drawing or deep drawing is performed [6–8].

This study addresses the effect of ultrasonic-vibration on hot upsetting. During the experiments, the ultrasonic-vibration frequency was 20 MHz, which is far from the ordinary natural frequency, 100 MHz, of a dislocation loop [10]; therefore, dislocations would absorb little energy of vibration due to the lack of resonance. Accordingly, dislocations would not make much effect on flow stress reduction. However, as shown in Fig. 2(b), during ultrasonic-vibration, the effect of compressive forces reduction was increased with the increase in the compression ratio. If the reduction of flow stress caused by ultrasonic-vibration was attributed only to the superposition of steady stress and alternating stress, then the compressive forces reduction must be a constant. Therefore, mechanisms other than the superposition of stresses should also be considered.

Fig. 7(c) shows that the magnitude of the reduction in force caused by ultrasonic-vibration decreases as the temperature is increased. The causes may be as follows: (1) The material's creep characteristic will gradually come to dominate at high temperature. The deformation mechanism therefore differs from that at room temperature. The ultrasonic-vibration energy absorbed by the material is reduced, weakening the effect of ultrasonic-vibration. (2) Ultrasonic-vibration increases the interface temperature between die and work-piece, and reduces the effect of the reduction in friction.

The experimental results indicate that the strain rate does not further reduce the material flow stress associated with ultrasonic-vibration. Currently, the developed ultrasonic-vibration system is limited to a relatively short operation time; only two strain rates were used during experiments; therefore, the connection between ultrasonic-vibration and strain rate effect has not been

well explored. A detailed study will be required in the future.

5. Conclusions

This study established the ultrasonic-vibration hot upsetting system. By adopting a cooling mechanism, the system overcomes high temperature operation difficulty. The effects of temperature and strain rate during the ultrasonic-vibration upsetting of the aluminum alloy were investigated. Based on the results of this study, we conclude the following:

(1) During the hot upsetting process, the difference between the temperatures of the furnace and the work-piece was significant. Therefore, a device to heat the die was required to eliminate the difference between the temperature of die and the work-piece.
(2) An axial ultrasonic-vibration can reduce the deformation resistance in hot upsetting.
(3) The effect of ultrasonic-vibration on hot upsetting cannot be explained by a simple mechanism, such as the effect of interface friction, or superposition of stress, or the absorption by dislocations of the ultrasonic-vibration energy.
(4) The magnitude of the reduction of forming stress in ultrasonic-vibration hot upsetting decreases as the temperature increases.
(5) The strain rate does not markedly affect the reduction of the flow stress in ultrasonic-vibration hot upsetting.

Acknowledgments

The authors would like to thank the National Science Council of Taiwan, ROC for the grant NCS-92-2212-E-009-007, under which the investigation was undertaken. The authors would also like to thank the National Center for High-Performance Computing for its facility support.

References

[1] F. Blaha, B. Langenecker, Naturwissenschaften 42 (1955) 556.
[2] B. Langenecker, Effects of ultrasound on deformation characteristics of metals, IEEE Transactions on Sonics and Ultrasonics 13 (1966) 1–8.
[3] W. Kempe, E. Kroner, Dislocation damping of aluminum single crystals at room temperature, Zeitschrift für Metallkunde 47 (1956) 302–304.
[4] G.E. Nevill, F.R. Brotzen, The effect of vibrations on the static yield strength of a low-carbon steel, Proceeding-American Society for Testing Material, 1957, pp. 751–754.
[5] E. Lehfeldt, R. Pohlman, Influence of ultrasonic vibration on metallic friction, Ultrasonics 4 (1966) 178–185.
[6] T. Jimma, Y. Kasuga, N. Iwaki, O. Miyazawa, E. Mori, K. Katsuhiko, H. Hatano, An application of ultrasonic vibration to the deep drawing process, Journal Materials Processing Technology 80–81 (1998) 406–412.
[7] M. Murakawa, M. Jin, The utility of radially and ultrasonically vibrated dies in the wire drawing process, Journal of Materials Processing Technology 113 (1–3) (2001) 81–86.
[8] M. Murakawa, M. Jin, P. Kaewtatip, Utility of ultrasonic vibration applied to metal-forming processes, Advanced Technology of Plasticity (1999) 19–24.
[9] Z. Huang, M. Lucas, M.J. Adams, Influence of ultrasonics on upsetting of a model paste, Ultrasonics 40 (1–8) (2002) 43–48.
[10] A.H. Cottrell, Dislocations and plastic flow in crystals, Clarendon Press, Oxford, London, 1953.

Journal of Materials Processing Technology 140 (2003) 30–35

Journal of Materials Processing Technology

www.elsevier.com/locate/jmatprotec

Simulation of ultrasonic-vibration drawing using the finite element method (FEM)

Masahiro Hayashi [a], Masahiko Jin [a,*], Sutasn Thipprakmas [a], Masao Murakawa [a], Jung-Chung Hung [b], Yu-Chung Tsai [b], Ching-Hua Hung [b]

[a] *Department of Mechanical Engineering, Nippon Institute of Technology, 4-1 Gakuendai, Miyashiro-machi Minamisaitama-gun, Saitama 345-8501, Japan*

[b] *1001 Ta Hsueh Road, Heinchu 300, Taiwan, ROC*

Abstract

In ultrasonic-vibration drawing, wires are drawn while ultrasonic vibration is applied to a drawing die. Prior studies provide experimental proof that ultrasonic-vibration drawing reduces drawing resistance, improves lubrication and prevents wire breakage. In the future, ultrasonic-vibration drawing is expected to contribute to the drawing of difficult-to-draw materials and operations, such as shaped wires, ultrafine wires, and the wire drawing operation in semidry or dry condition. However, a detailed analysis and understanding of the mechanism of improvement is not possible on the basis of conventional experimental observations because the ultrasonic-vibration processing phenomenon occurs at high speed. Therefore, we attempted to understand the processing mechanism of ultrasonic-vibration drawing using the finite element method (FEM). ABAQUS was used for the FEM. Drawing force and stress–strain distributions in drawn wires were analyzed. From these studies, we quantitatively clarified the mechanism of improved drawing characteristics, such as decreased drawing force.

Keywords: Wire drawing; Ultrasonic vibration; Finite element method (FEM); Drawing force

1. Introduction

In recent years, the drawing of difficult-to-draw materials, such as various titanium alloys and inter-metallic compounds, or difficult-to-draw operations, such as processing of shaped wires used for glass frames and ultrafine wires for use in wire bonding are often required [1,2]. On the other hand, from the viewpoint of the reduction of environmental burden, the use of chlorine-free lubricant in the process, furthermore, semidry or dry process has been demanded [3].

Ultrasonic-vibration drawing has been considered as a means of accommodating these high-level drawing processes. This drawing method involves the application of ultrasonic vibration to either the axial or radial direction of the die during drawing. To date, it has been proven that this drawing method contributes to the improvement of lubricant conditions and the decrease in drawing force [4]. It is expected that the ultrasonic-vibration drawing method will be viewed as an effective means of resolving the issues discussed above.

Several studies have been conducted on this subject. Mori and Inoue [5] carried out the study to fabricate fine wires by the use of the axial direction ultrasonic-vibration drawing method. Sansome [6] studied on tube drawing by the radial direction ultrasonic-vibration drawing method. Murakawa et al. [7] realized chlorine-free skin-pass drawing of stainless steel wires by the application of the radial direction ultrasonic-vibration drawing method.

Some studies were attempted to analyze the mechanism of improved drawing performances, such as reduced drawing force and improved lubrication characteristics [8,9]. However, detailed and quantitative experimental analyses have not been performed because of the difficulty of real-time measurements of drawing phenomena during the application of ultrasonic vibration.

To overcome this difficulty, we carried out a quantitative study of the mechanism of improved drawing characteristics in ultrasonic-vibration drawing using FEM analysis. We used a program (ABAQUS) for the FEM and analyzed the drawing force and the stress and strain distributions in the wire.

* Corresponding author. Tel.: +81-480-33-7614; fax: +81-480-33-7645.
E-mail address: jin@nit.ac.jp (M. Jin).

0924-0136/$ – see front matter © 2003 Elsevier B.V. All rights reserved.
doi:10.1016/S0924-0136(03)00699-X

As a result of the study, it has become possible to quantitatively understand the mechanism of improved drawing characteristics such as reduced drawing force.

2. Results of experimental evaluation of relationship between drawing speed and drawing force in past study [8]

Fig. 1 shows the ultrasonic-vibration wire drawing mechanisms for (1) axial (ultrasonic) vibration drawing (AUD) and (2) radial (ultrasonic) vibration drawing (RUD), and the relationship between drawing speed and drawing force based on data that were obtained experimentally for conventional drawing (CD), AUD and RUD. In these experiments, the ultrasonic-vibration frequency (f) was 15 kHz, the amplitude (a) was 1 μm and the drawn wire diameter (d_w) was 6.0 mm. The material used was pure aluminum wire, A1070-H. The reduction ratio R was 6.6%.

The results indicate that drawing force was independent of drawing speed in the case of CD; i.e. it was constant at 620 N. On the other hand, the drawing force increased with drawing speed in the case of AUD. The drawing force is equal to that obtained for CD under the critical drawing speed condition (i.e. $V_c = 2\pi af = 93.6$ mm/s) at which the maximum ultrasonic-vibration speed is roughly equal to the drawing speed. On the other hand, in the case of RUD, the relationship between drawing speed and drawing force is similar to that obtained for AUD. However, the critical drawing speed condition (V_c) is expressed by $V_c = 2\pi af/\tan\alpha$; it was 890.5 mm/s at die half angle of $\alpha = 6°$ in the case of RUD. This is 9.9-fold higher than for AUD.

Generally, speaking, drawing force generated by AUD and RUD ultrasonic-vibration drawing is substantially small compared with that generated by CD. The drawing force reducing effect increases with decreasing drawing speed. Unfortunately, these experimental results do not represent real-time drawing resistance under ultrasonic-vibration conditions. In other words, ultrasonic-vibration frequencies used in drawing apparatus are generally two orders of magnitude higher than the natural frequencies of measurement systems. Therefore, we think that the measured drawing force indicates an average value of actual dynamic drawing force by the ultrasonic-vibration period. The difficulty of real-time measurement of drawing force remains unresolved.

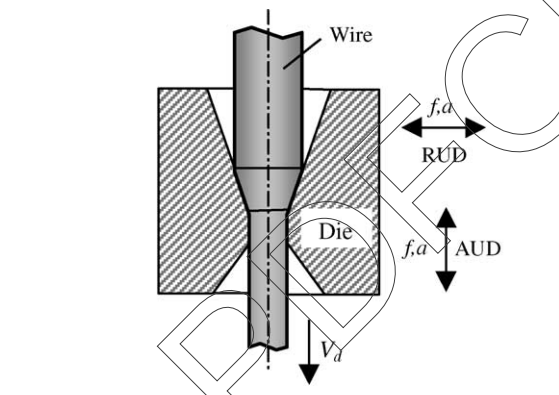

(a) Ultrasonic-vibration wire drawing mechanisms for AUD and RUD

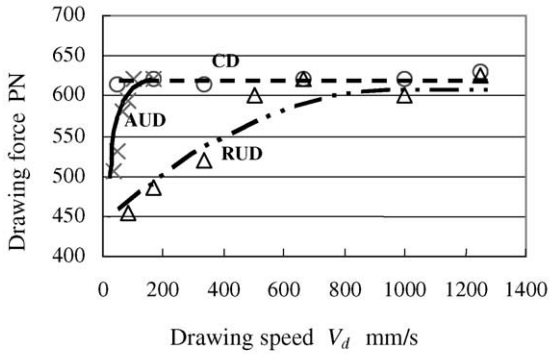

(b) Experimental results of relationship between drawing speed and drawing force

Fig. 1. Ultrasonic-vibration wire drawing mechanisms and relationship between drawing speed and drawing force in CD, AUD and RUD (Section 2).

3. FEM simulation method of ultrasonic-vibration drawing

Fig. 2 shows the FEM analysis model used in this study and Table 1 shows the conditions used in the analysis. "ABAQUS standard", a commercially available analysis code, was used in the analysis. The analysis is based on a

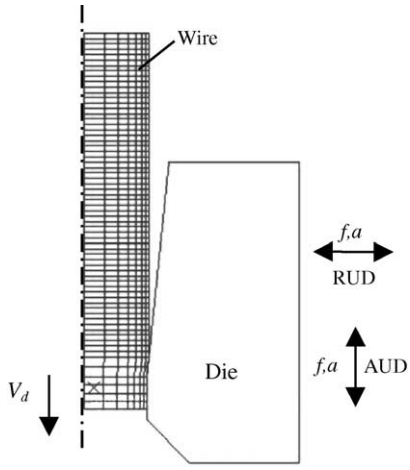

Fig. 2. FEM simulation model of ultrasonic-vibration wire drawing method.

Table 1
FEM simulation conditions

Wire	Elasto-plastic deformable body
Die	Rigid body
Simulation model	Axisymmetric model
FEM program	ABAQUS standard

Table 2
Material properties and drawing conditions

Wire drawing speed (V_d)	30–9000 mm/s
Wire material	Aluminum (A1070-H)
Young's modulus (E)	69 GPa
Yield strength (σ_y)	55.43 MPa
Poisson's ratio (ν)	0.33
Density	3.6 g/cm^3
Die material	Sintered carbide
Density	14.8 g/cm^3
Diameter of wire	Ø 6.0 mm
Diameter of die	Ø 5.8 mm
Reduction (R)	6.6%
Length of wire drawing (L)	16 mm
Friction coefficient (μ)	0.05

Table 3
Ultrasonic-vibration conditions

	Vibration direction	Frequency, f (kHz)	Amplitude, a (0-P) (μm)
CD	None	None	None
AUD	Axial direction	14.9	1, 10
RUD	Radial direction	14.9	1, 10

two-dimensional axial symmetry model. Analyses were performed for CD, AUD and RUD. In the simulation, the wire materials used for drawing were defined as an elasto-plastic body and the die as a rigid body.

Table 2 shows material properties and drawing conditions used in the analysis. The drawing conditions were set on the basis of the above experimental conditions; the diameter of the wire drawn (d_w) was 60 mm and it is pure aluminum, A1070-H. The die diameter (d) was 5.8 mm. The reduction ratio (R) was 6.6%.

Table 3 shows vibration conditions in ultrasonic-vibration drawing. The axial and radial vibration frequencies were $f = 14.9$ kHz. The amplitude was set to $a = 1$ and 10 μm.

4. Results of analysis and discussion

4.1. Relationship between drawing speed and drawing force

Fig. 3 shows the result of calculation of drawing force (P) at two different levels of drawing speed for the case of CD. In each figure, the abscissa and ordinate represent time and drawing force, respectively. The drawing force (P) was constant at approximately 620 N ($\sigma = 23.5$ N/mm^2) regardless of drawing speed (V_d). There was measurement fluctuation within 60–80 N which is considered to be caused by calculation error of FEM analysis.

Next, Fig. 4 shows the results of analysis for AUD, which is similar to the preceding analysis. In these studies, as shown in Fig. 4(a), the drawing force was within the range of 450 N ($\sigma = 17.0$ N/mm^2) to 670 N ($\sigma = 25.4$ N/mm^2) and

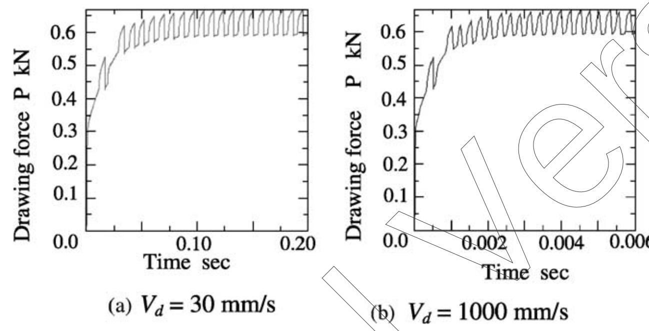

Fig. 3. Drawing force diagrams for CD analyzed by FEM (amplitude 1 μm).

fluctuated at the period of ultrasonic vibration (67 μs) when $V_d = 30$ mm/s, which is below the critical drawing speed. Fig. 4(b) shows details of the fluctuation period for drawing force. When the drawing speed is greater than the critical drawing speed, $V_d = 300$ mm/s, as shown in Fig. 4(c), the drawing force, P, was approximately the same as the value obtained for CD, 620 N ($\sigma = 23.5$ N/mm^2). This means that the drawing force fluctuation caused by ultrasonic vibration was eliminated.

Finally, similar analyses to those above were performed in the case of RUD; Fig. 5 shows the results. As shown in Fig. 5(a), the drawing force fluctuates within the range of 280 N ($\sigma = 10.6$ N/mm^2) to 580 N ($\sigma = 22.0$ N/mm^2) with a period of ultrasonic vibration of 67 μs at $V_d = 30$ mm/s. Next, drawing force P fluctuated within 400 N ($\sigma = 15.1$ N/mm^2) to 620 N ($\sigma = 23.5$ N/mm^2) at $V_d = 300$ mm/s. However, drawing force was almost the same as that observed in the case of CD, i.e. 620 N ($\sigma = 23.5$ N/mm^2) at $V_d = 1000$ mm/s.

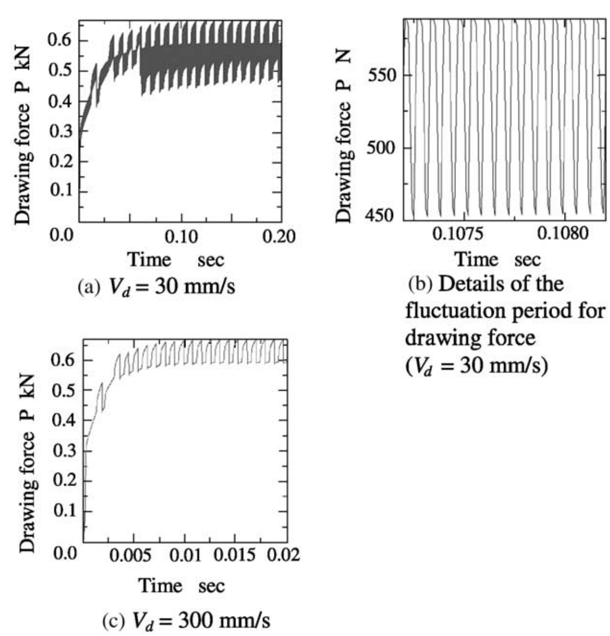

Fig. 4. Drawing force diagrams for AUD analyzed by FEM (amplitude 1 μm).

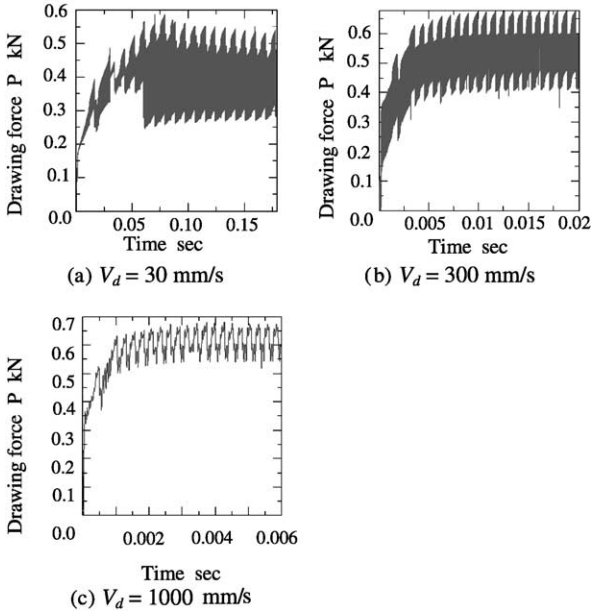

Fig. 5. Drawing force diagrams for RUD analyzed by FEM (amplitude 1 μm).

The above results can be summarized as follows. For both AUD and RUD, the drawing force fluctuated with a period of the die vibration when drawing speed was below the critical drawing speed and the fluctuation amplitude tended to increase with decreasing drawing speed. When drawing speed reaches the critical value, the fluctuation of drawing force disappears; the waveform is essentially the same as that observed in CD analysis.

4.2. Comparison of experimental and analytical results regarding the relationship between drawing speed and drawing force

As described above, drawing force measured by the experiments is considered to be the average value of the actual fluctuating drawing force owing to the ultrasonic vibration. Fig. 6 shows the relationship between drawing speed and

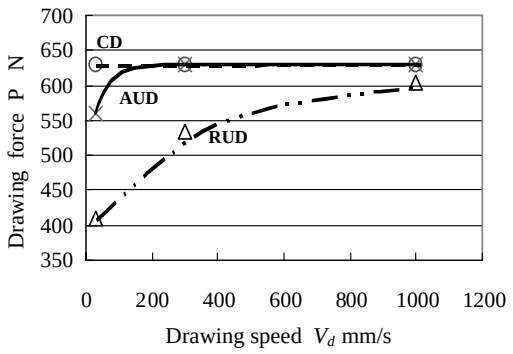

Fig. 6. Relationship between drawing speed and drawing force in CD, AUD and RUD (FEM simulation results).

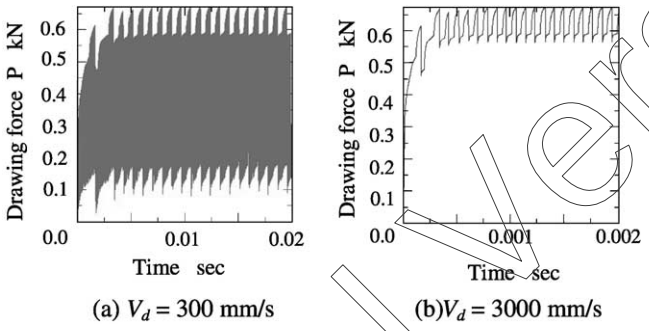

Fig. 7. Drawing force diagrams for AUD (amplitude 10 μm).

drawing force for CD, AUD and RUD. According to FEM analysis, the average drawing force in CD is independent of drawing speed and is essentially the same as that obtained in experiments. Drawing force is constant at 620 N. In the case of AUD, the profile of drawing force changed at the dividing point, which is the critical drawing speed V_d. The critical drawing speed is 93.6 mm/s in the case of AUD. The profile is similar to that obtained for CD when the drawing speed is at the critical speed or higher. On the other hand, the drawing force tended to approach zero with decreasing drawing speed when the drawing speed is lower than the critical speed. The drawing force tendencies for AUD and RUD were almost the same. However, the critical drawing speed of RUD is approximately 10-fold that of AUD.

In other words, the FEM analysis describing the relationship between drawing speed and drawing force in this study yielded the same results in this study as those obtained by conventional experiments.

4.3. Relationship between amplitude of ultrasonic vibrations and drawing force

According to the critical drawing speed concept, a large drawing force reduction can be obtained by increasing either the frequency or amplitude of ultrasonic vibration. These effects are seen under high-speed drawing conditions and are beneficial in terms of productivity.

Considering the above observations, we performed FEM simulations on drawing force waveforms for the case when the amplitude was set 10 times higher than the previous experiment (i.e. $a = 10$ μm). The reason for analyzing drawing force at high amplitudes is that it is easier to increase amplitude than to increase frequency due to the characteristics of ultrasonic-vibration devices. Furthermore, it is practical to obtain an amplitude (a) of 10 μm at a vibration frequency (f) of 15 kHz.

First, Fig. 7 shows results of drawing force obtained by FEM analysis for two levels of drawing speed for AUD. According to the results, the fluctuation of drawing force due to ultrasonic vibration improved approximately 10-fold compared with the results shown in Fig. 4.

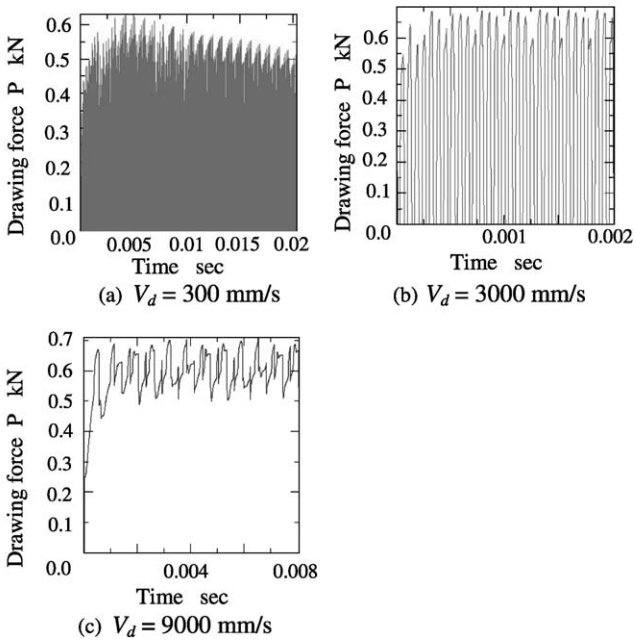

Fig. 8. Drawing force diagrams for RUD analyzed by FEM (amplitude 10 μm).

Next, Fig. 8 shows the results of FEM analysis of drawing force waveform for three levels of drawing speed in the case of RUD. Again, similar to the case of AUD, the fluctuation range of drawing force improved compared with the results shown in Fig. 5. In particular, the lower limit of drawing force was zero at drawing speeds (V_d) of 300 mm/s or less. This means that the die was completely separated from the wire. In other words, the hypothesis that drawing advances while the die and the wire repeat the process of contact and separation in RUD has been proven quantitatively by means of FEM analysis.

Fig. 9 shows the frequency-averaged drawing force for CD, AUD and RUD at an amplitude (a) of 10 μm. Thus, similar to the results discussed above with respect to Fig. 6, the drawing force decreases substantially and approaches zero when the drawing speed is less than or equal to the critical drawing speed for both AUD and RUD. Furthermore, FEM analysis predicted continuation of vibration effects up to the high drawing speed (V_d) of 8900 mm/s for RUD.

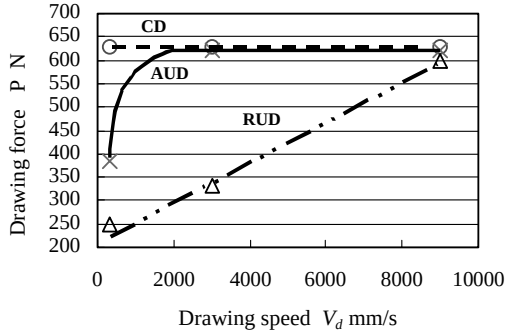

Fig. 9. Relationship between drawing speed and drawing force in CD, AUD and RUD (FEM simulation results).

4.4. Comparison of stress distributions in the wire drawn by the ultrasonic-vibration drawing method

Fig. 10 shows the stress distribution in the wire during drawing by CD, AUD and RUD. Fig. 10(a) shows the von Mises stress distribution for CD. The maximum stress value is found near the surface layer of the die-bearing section and maximum stress value is 146.7 MPa. On the other hand, as

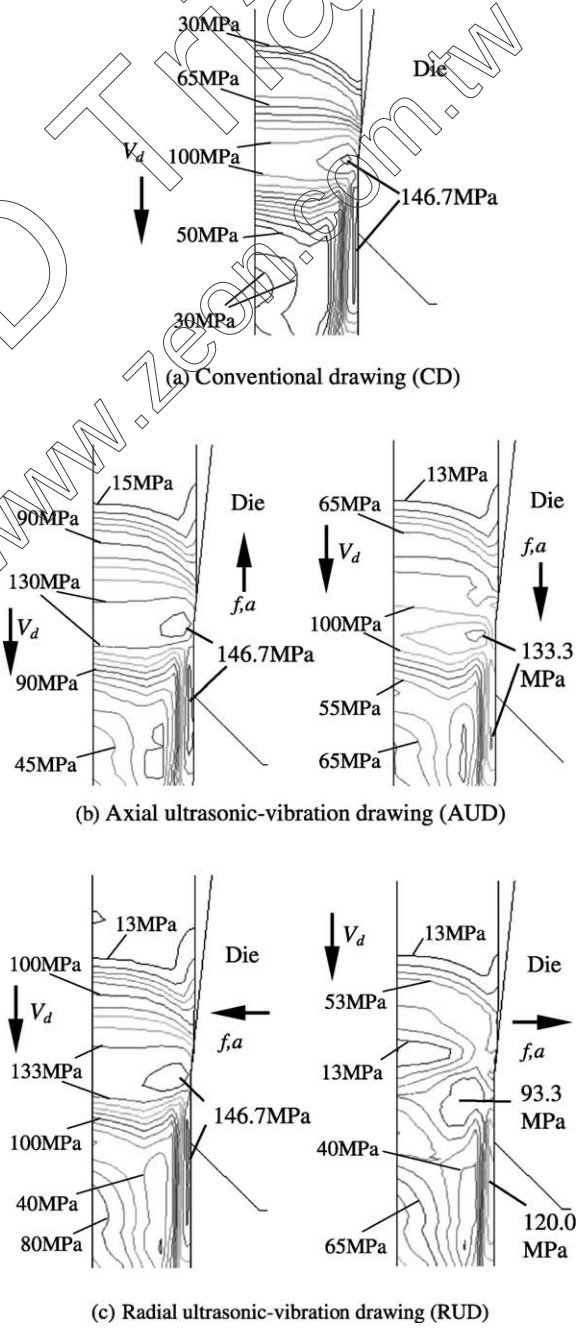

Fig. 10. von Mises stress distribution in the wire during drawing by CD, AUD and RUD (drawing speed 300 mm/s, amplitude 10 μm).

shown in Fig. 10(b), when the vibration direction of the die is opposite to the direction of drawing, the stress distribution was similar to that of CD in the case of AUD. However, when the direction of vibration is in the same direction as drawing, the maximum stress value decreased by approximately 91% compared to CD. As shown in Fig. 10(c), when the vibration of the die is directed to the center of the wire, the stress distribution for RUD is similar to that obtained for CD. On the other hand, when the direction of vibration is in the radial direction of the wire, the maximum stress value decreases substantially by 64%.

In both AUD and RUD, the maximum stress value in wires tended to decrease periodically. FEM analysis showed a tendency for a greater rate of decrease of the maximum stress value at higher amplitudes, in the case of RUD.

On the other hand, FEM analysis was performed on equivalent plastic strain distribution inside a drawn wire. There was no significant difference in equivalent plastic strain among CD, AUD and RUD.

5. Conclusions

We performed simulations using FEM on drawing force and stress–strain distribution of wires drawn by AUD and RUD. The simulations clarified the following points.

(1) For both AUD and RUD, it is possible to quantitatively analyze the drawing force waveform, which changes according to the period of ultrasonic vibration.
(2) The frequency-averaged values of fluctuating drawing force waveforms for AUD and RUD agree closely with results of drawing force measurements in conventional experiments.
(3) The critical drawing speed calculated by FEM analysis essentially agrees with the theoretical value obtained on the basis of the equality of the drawing speed obtained by conventional methods and the speed of vibration under maximum vibration amplitude conditions.
(4) FEM analysis quantitatively clarified the dependence of the reduction of drawing speed on amplitude.
(5) FEM analysis quantitatively revealed changes in stress distribution in wires.

Acknowledgements

This research was conducted as a joint study between Nippon Institute of Technology and Taiwan National Chiao Tung University. The two universities have a partnership as sister universities. We are thankful for the support extended by both universities. We thank Professor Kazuya Yoshida of the School of Engineering, Tokai University, Japan for his assistance with the drawing experiment.

References

[1] S. Norasethasopon, K. Yoshida, Finite-element simulation on wire breakage induced by eccentric inclusion in shaped wire drawing, Proc. School Eng. Tokai Univ. 27 (2002).
[2] K. Yoshida, M. Watanabe, H. Ishikawa, Drawing of Ni–Ti shape-memory alloy fine tubes used in medical tests, J. Mater. Process. Technol. 118 (2001).
[3] K. Seiji, Environmentally friendly lubricating technology in future, J. JSTP 43 (492) (2002) (in Japanese).
[4] L. Li, X. Lang, Wire drawing with ultrasonic vibration, J. Wire Ind. 61 (721) (1994).
[5] E. Mori, M. Inoue, Effects of drawing speed and backward tension application of ultrasonic vibration to metal wire drawing (2nd report). J. JSTP 11 (144) (1970) (in Japanese).
[6] D.H. Sansome, New developments in ultrasonic tube-drawing, Tomorrow Tube (1986).
[7] M. Murakawa, P. Kaewtatip, M. Jin, Skin pass wire drawing of stainless steel with chlorine-free lubricant with the aid of ultrasonic vibration, Trans. NAMRI/SME 29 (2000).
[8] M. Murakawa, M. Jin, The utility of radially and ultrasonically vibrated dies in the wire drawing process, J. Mater. Process. Technol. 113 (2001).
[9] Y. Meng, X. Liu, J. Chen, A dynamic contact model for ultrasonic wire drawing, Proc. ICTMP 1 (1997).